29A

Kapiti Coast Erosion Hazard Investigations: Waves, Tides, Storm Surge and Sea-level Rise

A.K. Laing
R.G. Bell
D.G. Goring
R.M. Gorman
S.J. Reid
J.A. Renwick

Prepared for

J. Lumsden, Coastal Engineering Consultants

Kapiti Coast District Council

Information contained within this report should not be used without the prior consent of the client

NIWA Client Report: LUM01301/1
Report WLG2000/59
December 2000

National Institute of Water & Atmospheric Research Ltd
PO Box 14-901, Kilbirnie, Wellington
New Zealand
Tel: 04 386 0300
Fax: 07 386 2153

CONTENTS

Reviewed by:

Lionel Carter
Principal Scientist, Physical Oceanography

Approved for release by:

Fred Smits
Business Development Manager

Document formatting approved by: P. Bradley or K. MacLeod, NIWA

Executive Summary

NIWA was commissioned by J Lumsden (Coastal Engineering Consultant) and Kapiti Coast District Council (KCDC) to undertake studies of wave conditions, tides, storm surge and sea-level along the Kapiti Coast.

Wave conditions off the Kapiti Coast have been assessed and new information generated by modelling the local wave growth. A 20-year record was synthesised from a time series of representative winds. Corresponding time series for ten shallow water sites along the coast were inferred by applying a refraction model.

Wave heights rarely exceed 3 m. The highest deep-water significant wave height estimated for waves off the Kapiti Coast was 4.5 m in early November 1995. Waves refract into the coast and a large proportion of their energy reaches the 10-m isobath. Swell from Cook Strait and the Tasman Sea may reach the Kapiti Coast, but it is substantially attenuated, with less than 15% of the energy reaching the coast.

A programme is recommended for measuring waves and currents near the shore. Such data are required to verify the local wave conditions, and to quantify longshore drift. This would be best served by deploying an S4 current meter for at least 6 months in about 10m water off the most vulnerable location (Raumati).

Analyses of known historic storm events, a 3-year sea-level record from Kapiti Island and nearly 30 years of barometric pressure data from Paraparaumu Airport have also been completed. The lowest recorded barometric pressure of 973 hPa would have produced an inverted barometer set-up of just over 0.4 m due to pressure alone. The highest observed storm surge was 0.7 m set-up accompanied by a 2.6 m wave set-up and run-up in the 11–13 September 1976 storm. During this event the estimated H_s offshore reached 3.6 m with a peak period of 9.4 s.

The highest predicted high tide for next 100 years will be 1.27 m above Wellington MSL Datum (1953). The tide range reduces as one moves south along the Kapiti coast, so high tides to the north (Otaki Beach) need to be scaled up by as much as 112% and those to the south (Pukerua Bay) need to be scaled down to as little as 68%.

Design sea-level set-up for 50-year return period and 100-year return period scenarios are estimated to be 3 m and 3.5 m respectively above Wellington MSL Datum (1953) for Waikanae Beach. An additional factor for wave run-up needs to be included on a site-by-site basis, plus the tidal range factor for beaches north and south of Waikanae Beach. No account has been included for a predicted increase in windiness over the next 100 years.

The interannual (year-to-year) elevation of background sea level at Kapiti could peak at +0.15 m for a month or so during strong La Niña episodes and warmer summer months. For the purposes of a combined design storm-surge event, a nominal +0.1 m set-up should be added to the design levels for both the 50-year and 100-year return periods. While ENSO episodes are not expected to change significantly, the global circulation models are predicting a 15% increase in windiness for the next 50 years, and by another 15% for 50 years after that. What effect this will have on the magnitude and frequency of extreme storms is still unclear.

There is a 50% chance that sea level around New Zealand will rise by +0.20 m by 2050 and by +0.45 m by 2100, according to the 1995 IPCC estimates. Forthcoming IPCC projections (due out in March 2001) are unlikely to recommend any lower rates of sea-level rise due to greenhouse effects.

1. INTRODUCTION

NIWA was commissioned by Kapiti Coast District Council (KCDC) in June 2000 to carry out studies of wave conditions, tides, storm surge and sea-level along the Kapiti Coast. The studies are to provide technical information for further work on the causes and scale of erosion along the coast, so that robust coastal management policies can be developed.

The scope of the present work is to review existing information on waves, tides, storm-surge and sea level, and to synthesise additional information on wave and storm-surge as necessary, so that there is a sound base of information for erosion studies, and assessing the erosion hazard.

2. WAVE ACTIVITY

2.1 Background

Wave action provides the energy which suspends sediment, leading to erosion or accretion of the shoreline. The effect of waves will vary according to the type of sediment on the beach or in the near-shore zone and the nature of the waves themselves.

A surface wave is associated with orbital motions of water "particles" in the water column beneath it. In deep water these motions are circular, decreasing in amplitude with depth. Where the wave "feels" the bottom they are elliptical, becoming more horizontally elongated nearer to the seabed. The amount of motion at the seabed is determined by the depth of the water and the period and height of the waves. Longer waves (with higher period) penetrate further and generate more action near the bottom. High waves are associated with more turbulence and vertical mixing. The angle of approach of the waves is also important in determining alongshore drift.

As a wave approaches the shore it will interact with the seabed. This has three major consequences:

- **shoaling** of the wave, where the forward motion of the wave is slowed, but since the energy flux is conserved, the wavelength shortens, the wave height increases and the wave steepens. The wave period remains the same.

- **refraction** of the wave, where, in an oblique approach, one part of the wave is in shallower water than another. The wave speed is dependent on the depth, so the wave bends towards the coast.

- **dissipation** of wave energy, as friction with the bottom extracts wave energy, diminishing the wave.

The depth of the water and the sea level are critical. Hence the impact of the waves on the coast will vary according to the state of the tide, or other factors affecting the sea level, such as storm surge. It is the combination of the sea level with wave action which determines the risk to the foreshore.

The wave field at any location spans a spectrum of wavelengths (periods) and directions. For waves generated in a single fetch, this spectrum is normally focussed around a

- **peak period (T_p)**, and
- **mean direction.**
- **The significant wave height (H_s),**

formally defined as the average of the highest one third of waves, is the standard parameter used to represent the characteristic wave height. In deep water the maximum height observed in any period longer than 3 hours will normally be just under twice the significant wave height. The

- **zero-crossing period (Tz)**

is the average period of waves, where a wave is the section of record between consecutive up/down crossings of the local mean sea-level datum.

2.2 Historical wave data

Observations

Ships of opportunity make regular visual observations of wave conditions and record these as part of the meteorological reports. Whilst these observations are individually of variable quality (Laing 1985), large ensembles give a good idea of the wave climate (Reid and Collen, 1983). Unfortunately wave conditions are expected to vary considerably from place to place within the region. Fetches are limited by the geography and the wind direction and speed varies from the outer regions near Farewell Spit to the inner Cook Strait. Hence, there is no sufficiently large group of observations representative of any individual location to make accurate assessments from these data.

An analysis of 25 years of these data indicates that, for the area between 40°S-41°S and 174°E-175°E, the significant height exceeds 3 m in 16% of the observations. However, this area includes a region in its west where strong south-easterly winds force waves to this level 5% of the time, and where westerly exposure is greater than at the coast. Hence this incidence of 3-m waves will be higher than at the coast, especially off the Kapiti Coast. It is expected that waves near Kapiti Island exceed 3 m rarely.

Harris (1990) made a summary of wave conditions in the greater Cook Strait area. For his region 6 (the Manawatu-Wanganui coast) the information was largely based on two measurement sites noted below. He also pointed out that considerable diminution of westerly swell is to be expected along this coast.

Satellite data also enable wave heights to be determined. These provide profiles of H_s along the sub-satellite track. Collations of the data are an accurate source of wave climate information. For deep water around New Zealand, Laing (2000a) has compiled such a climatology. Unfortunately, as with the ships' observations, such climatologies do not have sufficient spatial resolution to be of value in complex coastal regions such as the South Taranaki Bight and Cook Strait.

Measurements

On the Kapiti coast there are no substantial records of measured wave data. This poses a significant problem in assessing the wave hazard to the coast. The nearest measurements of any substance were made further up the coast at Himitangi (40.373°S,175.193°E, see Figure 2.1) in 30 m of water over a 3-month period in summer 1986-87. A one-year record from near Wanganui (20.001°S, 174.091°E) was measured at a similar from January 31, 1986 to February 25, 1987 (Macky et al., 1988). Although these sites have different exposures, they are reasonably similar in that most of the wave energy will be derived from the same events that affect the Kapiti Coast. The exposure to the open ocean beyond Farewell Spit and Taranaki is similar in breadth but from a different angle. Since swell off the west coast of New Zealand is predominantly from the southwest quarter, it will affect the northern sites more than the Kapiti Coast. Further, the fetch in local southerly winds is different. Some Cook Strait waves will affect the Kapiti Coast. These will not reach much further up the coast but locally driven waves off Manawatu will affect the Wanganui site.

Comparison of H_s from the Wanganui and Himitangi measurements shows a general similarity. The same events affect both sites but the waves at Wanganui are about 20% higher than at Himitangi (Macky et al. 1988). The same events are expected to affect waters off the Kapiti Coast (beyond Kapiti Island), but wave heights are likely to be lower than at Himitangi.

The median H_s measured at Wanganui was about 1.1 m and the modal T_z was 5.5 s. H_s exceeded 3 m only 1.6% of the time and the maximum measured H_s was 4.5 m. Macky et al. (1988) also made extreme wave estimates for the site, deriving an expected 5% annual exceedence threshold of 7.4 m. It is emphasised that near Kapiti Island there is less exposure to substantial fetches, waves are expected to be lower and it is expected that H_s rarely exceeds 3 m.

Further afield an 11-year measured wave record exists for the Maui-A oil and gas production platform (Kibblewhite et al. 1982, Ewans and Kibblewhite 1990). However, this site is exposed to a quite different wave regime from the Wanganui-Manawatu-Horowhenua-Kapiti coast. Southwest swells are persistent at Maui but only sporadically refract to penetrate the South Taranaki Bight and reach the measurement sites or the Kapiti Coast. The Maui site also suffers many energetic events from the south-east, which are offshore along the coast in question and therefore have little effect on the local wave climate.

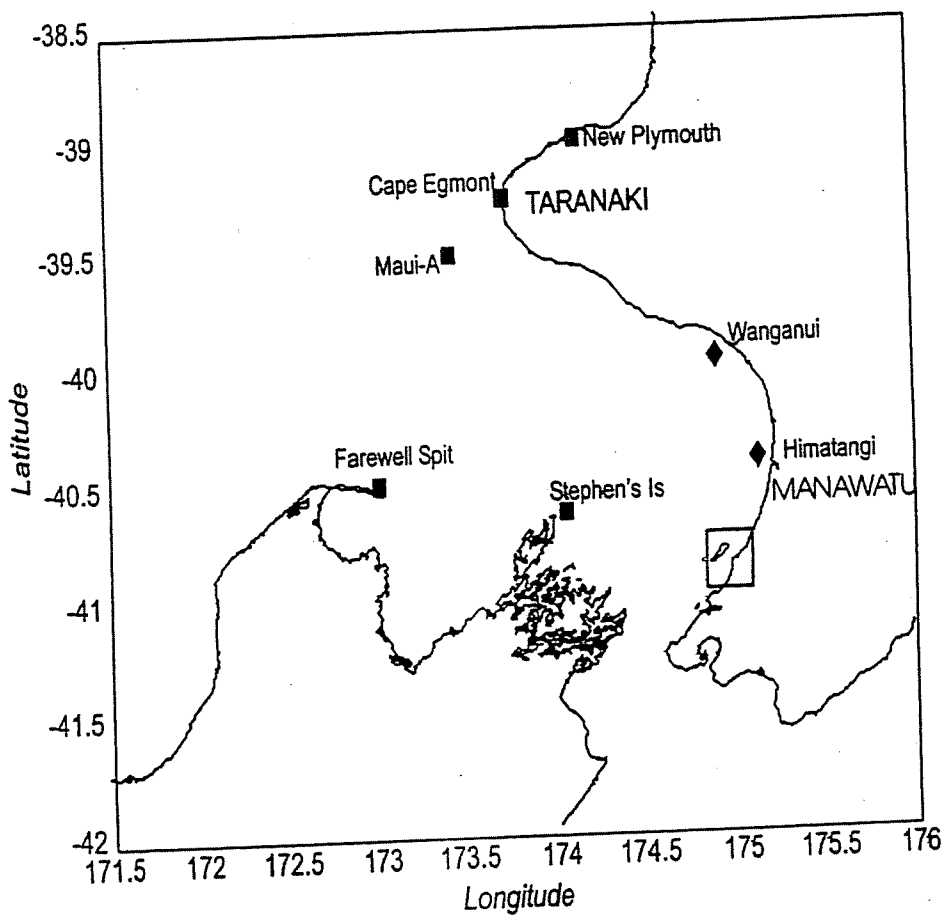

Figure 2.1: The wider study area showing sites of meteorological observations (squares) and wave measurements (diamonds). The smaller area around Kapiti Island is expanded in Figure 2.10

2.3 Synthesising a wave record

In the absence of local measurements a synthetic record has been generated. There are two approaches to this. The first would be to implement a numerical wave model over the whole region, driven by winds derived from a numerical prediction model. Such a model (WAMDIG, 1988) has been applied to the New Zealand region (Gorman and Laing, 2000, Laing and Gorman, 2000) using a database of 15 years of wind fields carefully reanalysed by the European Centre for Medium-range Weather Forecasts. This application has derived useful results for open coasts around New Zealand. However, such modelling is complex, and would require careful attention to the wind fields used to generate the waves. Since the wind fields in the region are complex, this would in turn require a high-resolution atmospheric model to be run over an extended period.

The alternative, simpler method used in the present analysis is to use meteorological observations of pressure and winds to estimate a representative wind in the fetch area critical to the target site. A simple parametric model is then applied to deduce wave parameters.

2.4 Determining the winds

Representative winds over the region between Taranaki, Farewell Spit and Kapiti Island were estimated for the years 1975 – 1995.

The time series are formed from 5 sets of measurements:

- ***Pressure data at New Plymouth, Farewell Spit and Paraparaumu.*** These stations provide mean pressure gradients from which geostrophic wind speed and direction were calculated. There is a reasonable coverage of data over the whole period except for 1992 and 1993 when there was a gap in the New Plymouth data. The mean speed for the entire period was about 11 ms^{-1}.

- ***Winds at Cape Egmont*** were reported systematically until 1986. The lighthouse was then closed. The mean speed for the period from 1975 was about 7 ms^{-1}.

- ***Winds from the Farewell Spit*** automatic weather station were available from 1980. The mean speed was a little below the Cape Egmont speed and increased over the data period.

- ***Maui winds*** are available from 1979 and are similar to the geostrophic speeds. Variations from year to year are similar to the geostrophic speeds.

- *Stephens Island* had the most broken record. The data from this station was treated with caution.

The measured wind data were matched up time for time against the geostrophic winds. Where these are missing in the period 1992-1994, the Farewell Spit data is used as the basic set. Gaps are left where one of the matching sets does not have a data value.

For the complete dataset annual means were calculated for each station. Where fewer than 500 data are available over an annual period the annual mean is not used. The resulting series of means are plotted in Figure 2.2.

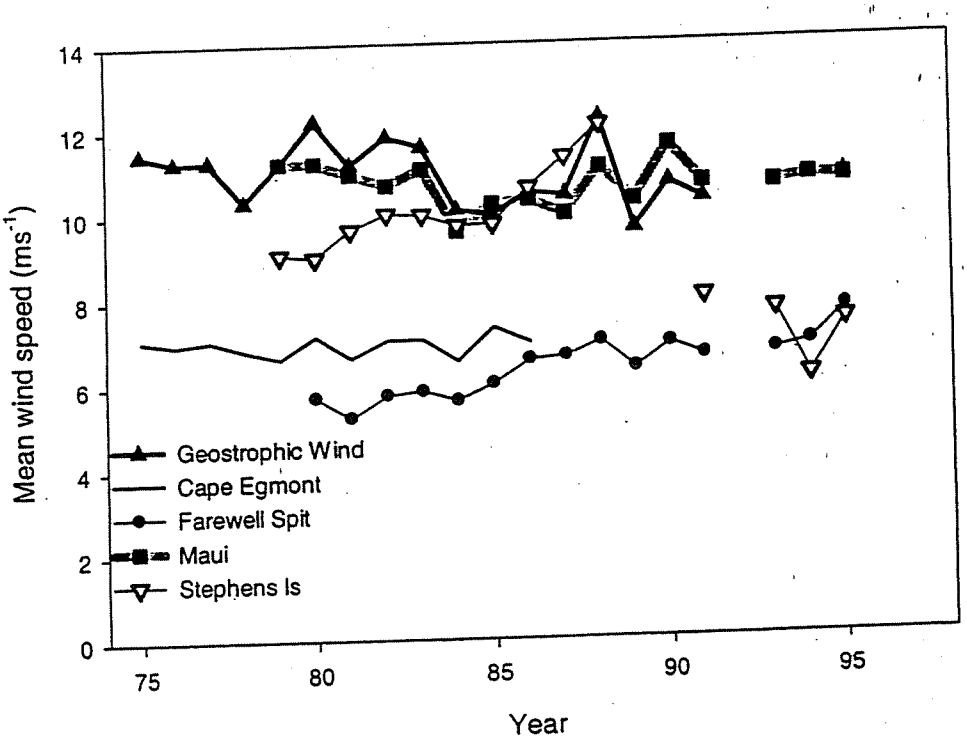

Figure 2.2: Annual means of wind speeds. The series are for geostrophic winds calculated from pressure measurements at Paraparaumu, New Plymouth and Farewell Spit, and wind observations at 4 sites in the primary area of influence for the Kapiti Coast.

The Maui winds are from measurements at about 80 m above the sea surface. A logarithmic reduction to 10 m (roughness length = 0.0002 m) requires multiplication of the speeds by 0.825.

The geostrophic winds represent winds above the marine boundary layer, and these are multiplied by the same factor. For consistency, the Farewell Spit and Cape Egmont winds are adjusted by a factor of 1.3 so that mean speeds of the four data sets are similar. The Stephens Island wind speeds are not used further and are not adjusted. The final series of winds is obtained by taking the mean of the adjusted datasets.

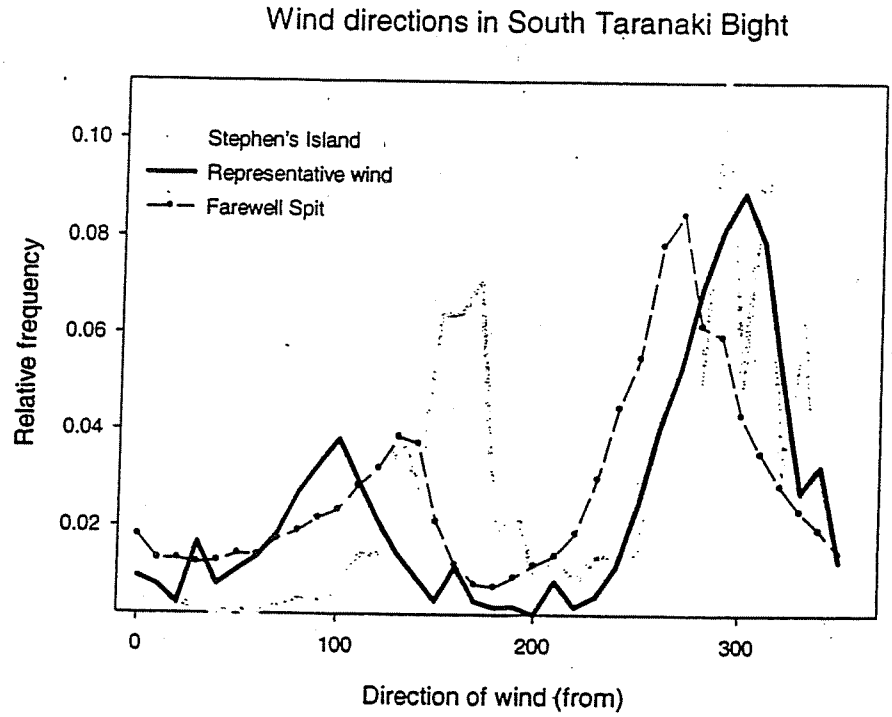

Figure 2.3: Relative frequency of wind directions for the derived representative data set, with the measured data from Farewell Spit and Stephen's Island.

The distribution of wind directions is shown in Figure 2.3. It shows all the characteristics expected of winds in the area. The northwesterly peak coincides with that at Stephen's Island and is slightly more northerly than that at Farewell Spit. The southerly peak is more easterly than both Farewell Spit and Stephen's Island.

Winds in the greater Cook Strait area have also been modelled using the Regional Atmospheric Modelling System, RAMS (Pielke et al., 1992). These help show the critical fetch for a typical strong northwesterly flow.

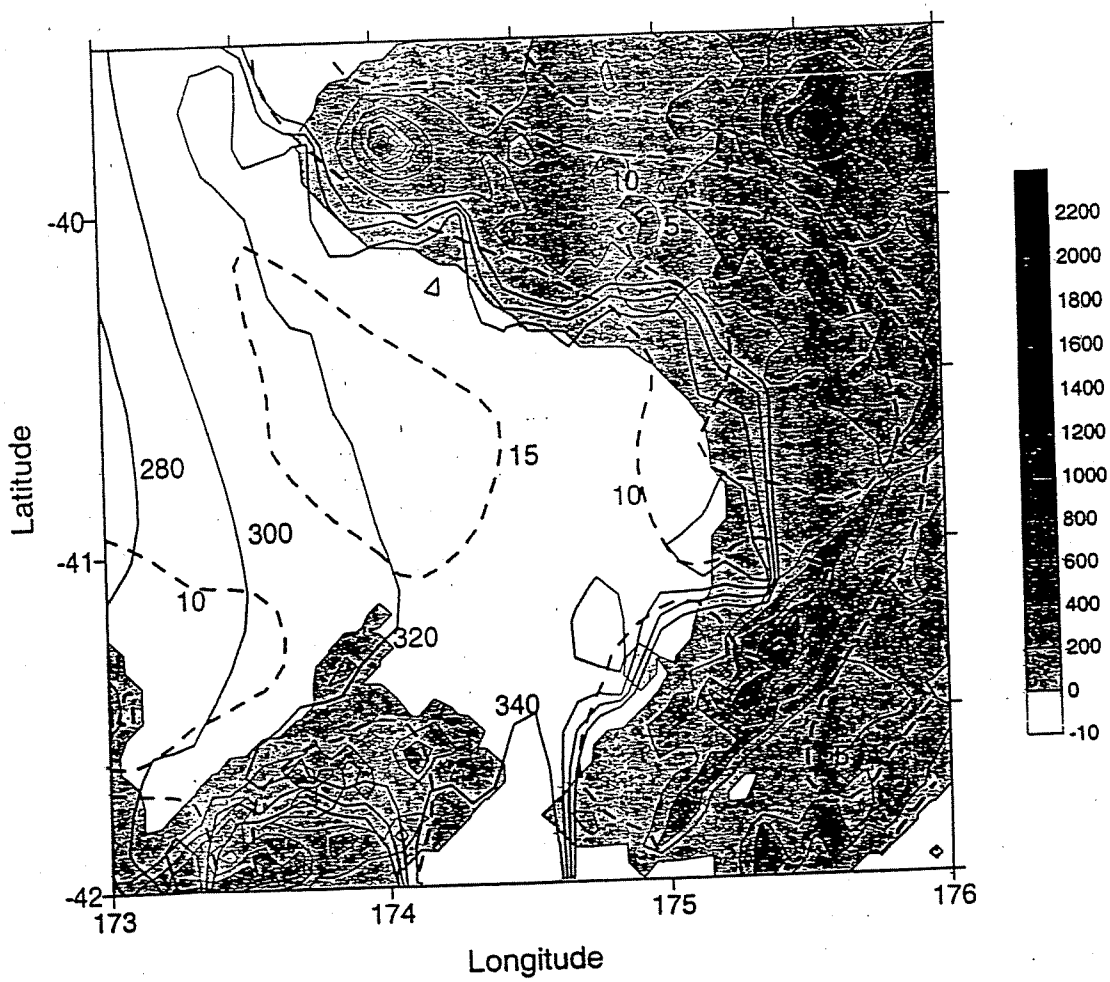

Figure 2.4: A RAMS simulation at 20 km grid resolution of the wind field over the Manawatu Bight at 6 pm on 15 Nov 1997 – a typical strong northwesterly. Shading according to elevation as shown on the accompanying scale shows the land form. The winds are for the lowest RAMS level at 95 m above MSL. The wind direction contours are solid lines at 20° intervals. The wind speed contours are dashed and at 5 ms^{-1} intervals. The directions gradually turn in a clockwise manner as the flow approaches Cook Strait and also change quickly near the coasts. The most constant fetch is from the south Taranaki coast to the Manawatu coast.

Figure 2.4 indicates that there is a region of reasonably constant wind direction between the South Island and Taranaki, but wind directions change quickly at the coasts. Wind speeds are strongest in the waters north of d'Urville Island. The most constant fetch is from the south Taranaki coast to the Manawatu coast.

Some idea of the extent of wind events can also be obtained from satellite-derived wind fields. These have been shown to be quite useful for depicting wind features in waters around New Zealand (Laing, 1994, Laing and Brenstrum, 1996). In Laing (1994) the corridor between Farewell Spit and Taranaki was shown to have reasonably uniform winds in westerly conditions, with a peak flow near the centre of the cross-section. Although the satellite data do not return waves within 25 km of the coast, the

general patterns observed in the greater Cook Strait area are of considerable value in determining the extent of fetches which will generate waves affecting the Kapiti Coast. In Figure 2.5 there is an increase in wind speed in the greater Cook Strait, consistent with the RAMS simulation shown in Figure 2.4.

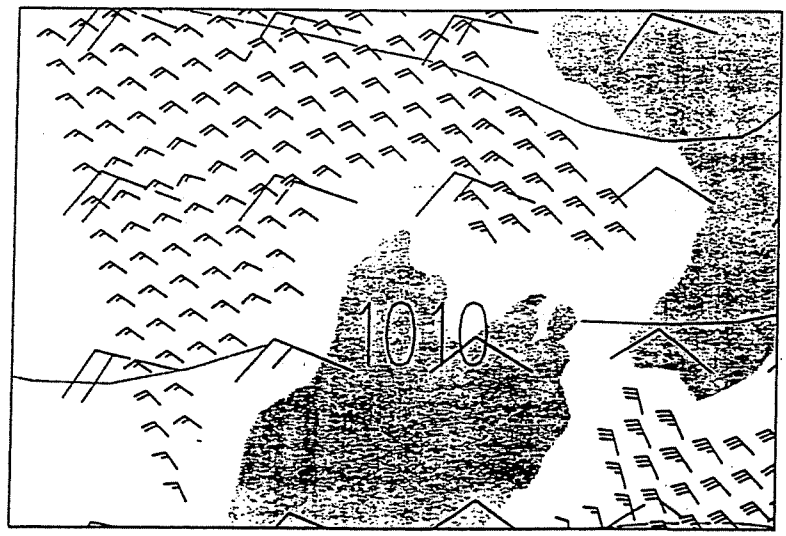

Figure 2.5: ERS-1 scatterometer winds for February 8, 1992, a typical north-west wind situation. The wind barbs show the wind speed in knots, with a full barb representing 10 knots and a half-barb 5 knots. The large wind barbs are winds from a global numerical model, and the contour lines are isobars (hPa) from the model surface pressure field.

From the wind observations, the model data and scatterometer data, the maximum practical fetch for the open ocean window has been established as 200 km. Otherwise, the fetch is limited by the local geography.

The duration of a wind event was determined directly from the constructed time series. An initial duration of 3 hours was set; the time-step in the data series. If the next value for the wind increased more than 3 ms^{-1} or changed direction by more than 30° then the duration was reset to 3 hours. Otherwise, the fetch was under the same wind regime and the duration was increased by 3 hours. Maximum duration was 24 hours.

2.5 Wave generation

For wave generation a simple parametric model based on limited fetch and limited duration has been used. Fetch-limited growth is determined from results of the JONSWAP (Joint North Sea Wave Project) study (Hasselmann et al. 1973). Hasselmann et al. (1976) developed a parametric model based on the JONSWAP

results, relating non-dimensional total energy $\tilde{E} = \frac{g^2 E}{U^4}$ to the non-dimensional fetch $\tilde{X} = \frac{gX}{U^2}$, for total energy E, fetch X, gravitational constant g and windspeed U:

$$\tilde{E} = 1.6 \times 10^{-7} \tilde{X} \quad (2.1)$$

The significant wave height $H_s = 4\sqrt{E}$.

For duration-limited growth the parameterisation used by Laing (2000b) has been adopted. This gives a simple exponential growth rate. It is couched in terms of the non-dimensional total energy $\tilde{E}$, and non-dimensional duration $\tilde{t} = \frac{gt}{U}$, where t is duration (s). The growth rate assumes neutral stability in the lower atmosphere. The form is:

$$\tilde{E} = 1.58 \times 10^{-9} \tilde{t}^{1.4}. \quad (2.2)$$

The smaller of the fetch-limited or duration-limited values is used.

Where the fetch is bordered on one side by land the directional spread of the waves has to be considered. A cosine-squared angular distribution is assumed, centered on the wind direction. Wave energy is reduced appropriately, depending on the arc of exposure of the site to the active fetch. This is achieved by defining an angular spreading factor for each direction, and applying it to the estimates of Hs derived from equations 2.2 and 2.3.

Wave period information is deduced from the JONSWAP relationships, with the peak period

$$T_p = 6.76 H_s^{-0.6} U^{0.2}. \quad (2.3)$$

2.6 Model validation

The wave data available for the site near Wanganui gives an opportunity to verify the model during a one-year period. The configuration of fetch and angular spreading factors were set for the wave measurement site described in Macky et al (1988).

Time series of the derived waves for spring 1986 are shown in Figure 2.6. Although H_s is reduced to zero in between events, a situation which arises from setting the wind speed to zero when it is blowing offshore, the series compares very well to the time

series shown in Macky et al. (1988). The magnitude of events reaching 3m is the same. The only events which may be missed are those where significant (2 m) swell penetrates from the Tasman Sea. This problem is expected to be less of a concern on the Kapiti Coast.

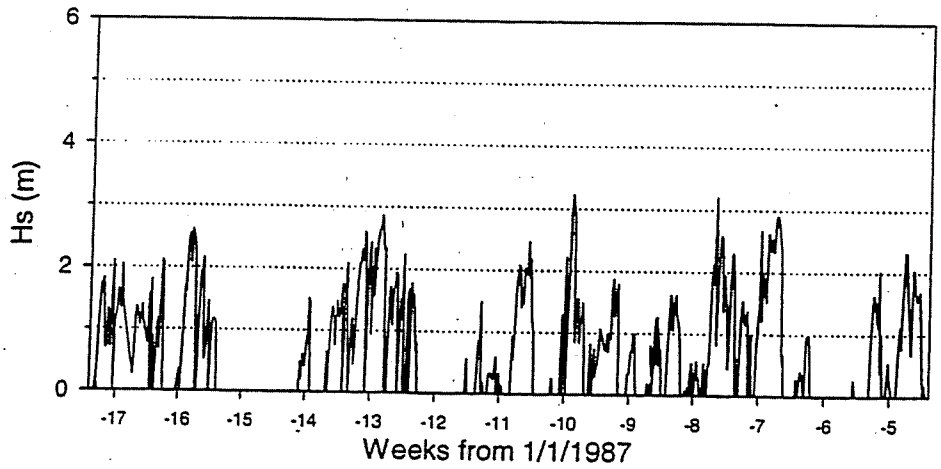

Figure 2.6: Simulated wave conditions off Wanganui, showing the significant wave height estimates (H_s) during spring 1986. The time period matches figure 6 in Macky et al. (1988).

The distribution of wave heights also matches that for the Wanganui measurements (see Figure 2.7 and Figure 9 of Macky et al., 1988). For example, simulated waves in the 2.5 m – 3.0 m range occur 3.9% of the time compared to 3.7% of the time for the measurements, and the highest simulated H_s of 4.53 m is very close to the highest measured value of 4.3 m.

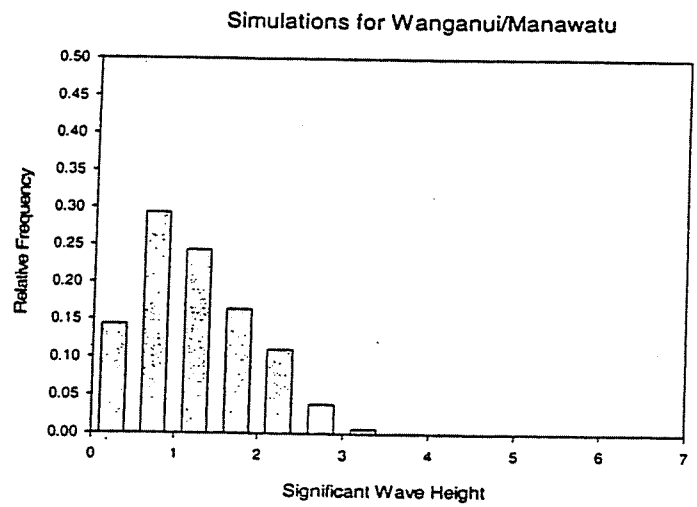

Figure 2.7: Relative frequency of simulated wave heights off Wanganui (see Figure 9 of Macky et al., 1988). Waves under 0.25m have not been included.

2.7 Waves off the Kapiti Coast

The model was then reconfigured and applied to a deep-water site just off Kapiti Island. A few modifications were made to cater for southerly winds in Cook Strait. Since winds from south of about 120° are forced through Cook Strait as southerlies, these were realigned to come from a direction of 220°. However the fetch in this direction was limited to 80 km.

A time series of wave parameters were derived for the full 20-year period. The record is provided electronically as one of the outputs of this contract. The distribution of wave heights is shown in Figure 2.8.

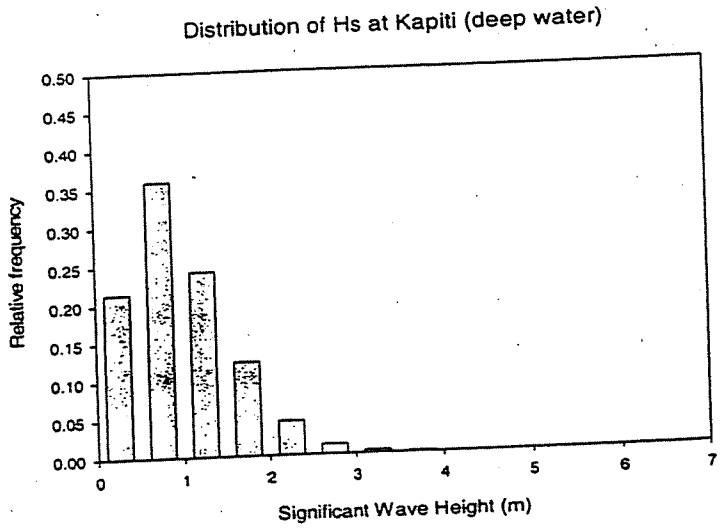

Figure 2.8: Relative frequency of simulated wave heights off Kapiti Island

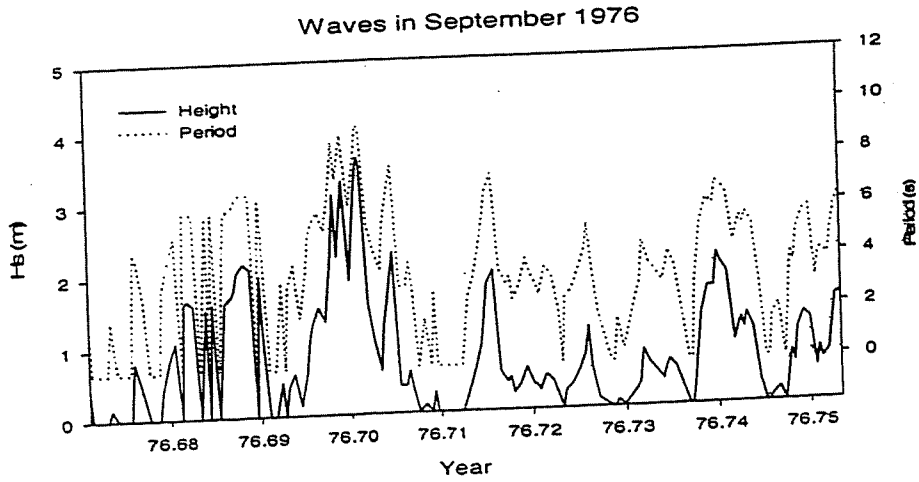

Figure 2.9: Simulated significant wave height (solid line) and peak period (dotted line) during September 1976. Year 76.10 corresponds to September 11, 1976.

The highest deep-water significant wave height was 4.5 m in early November 1995, followed by 4.1 m in March 1995. During the major event of 11-13 September 1976, H_s reached 3.6 m with a peak period of 9.4 s. Figure 2.9 shows the wave height and period record for that month. The significant wave height exceeded 3 m only 0.3% of the time.

2.8 Waves at the coastline

Waves from deep water near Kapiti Island were translated to 10 different sites along the Kapiti Coast. This procedure used a refraction model, WBEND, which applies the appropriate shoaling, refraction and dissipation to waves with given period and height approaching from a given direction.

The wave refraction model WBEND

Model WBEND (Black and Rosenberg, 1992a, Black, 1997) is a 2-dimensional numerical wave refraction model for monochromatic waves or a wave spectrum over variable topography. The model applies a fast, iterative, finite-difference solution of the wave action equations to solve for wave height, wave period, breakpoint location and longshore sediment transport.

WBEND simulates refraction by solving the wave action equation for the conservation of wave power in two dimensions given by

$$\frac{\partial}{\partial x}(F\cos\theta)+\frac{\partial}{\partial y}(F\sin\theta)=-F_D\,, \tag{2.4}$$

where x and y are orthogonal co-ordinates, θ is the wave angle and F_D $(= F_f + F_b)$ is a combination of the bed friction (F_f) and wave breaking (F_b) dissipation terms. F is the wave power which, for Airy waves, is

$$F = EC_g = \frac{1}{8}\rho g H^2 C_g$$

where E is the wave energy, C_g is the group speed, ρ is the fluid density, g is gravitational acceleration and H is the wave height.

The wave angle is obtained from the equation for conservation of wave number

$$\frac{\partial}{\partial x}(|k|\sin\theta)-\frac{\partial}{\partial y}(|k|\cos\theta)=0\,. \tag{2.5}$$

The model solves equations 2.4 and 2.5 for wave power and wave angle respectively using a shoreward marching iterative scheme (Black and Rosenberg, 1992b). Height and angle are directly obtained on a regular finite difference grid, which eliminates the need for interpolation, as required when a ray tracking procedure is used.

To obtain the wave number k, the dispersion relation for linear waves,

$$\omega^2 = gk \tanh(kh)$$

is solved using an iterative *Newton-Raphson* technique, given the radian frequency ω and depth h.

A formulation based on the horizontal eddy viscosity in the hydrodynamic model 3DD (Black, 1995) is used to smooth the height and angle solutions. This has the effect of spreading energy along the wave crests, similar to the process of diffraction. While solving the wave action and conservation of wave number equations, heights and angles are smoothed by the function ψ given by,

$$\psi = \varepsilon \frac{\partial^2 \varphi}{\partial y^2}$$

where ε is the eddy viscosity coefficient and φ is either wave height or angle. The dominant wave direction is along the model's x-axis, and so the term acts primarily along the wave crests. The eddy viscosity coefficient is set by calibration. Simulations of several different environments (e.g. Black and Rosenberg, 1992a,b; Hutt, 1997; McComb et al., 1997) have indicated that appropriate values are in the range $0.02 < \varepsilon < 0.06$.

For monochromatic cases, the wave-energy frictional dissipation term is given by,

$$F_f = \frac{\rho C_f}{6\pi} \left(\frac{H\omega}{\sinh(kh)} \right)^3$$

where C_f is the friction coefficient.

Wave breaking is assessed by checking if height exceeds a depth limitation, that is if $H > \gamma h$, where γ is user selected and is typically of order 0.6-0.8.

Kapiti Coast refraction modelling

The refraction model was applied to determine wave conditions at 10 inshore sites (see Table 2.2, and Figure 2.10), located in 10 m and 20 m water depth offshore from 5 beach locations.

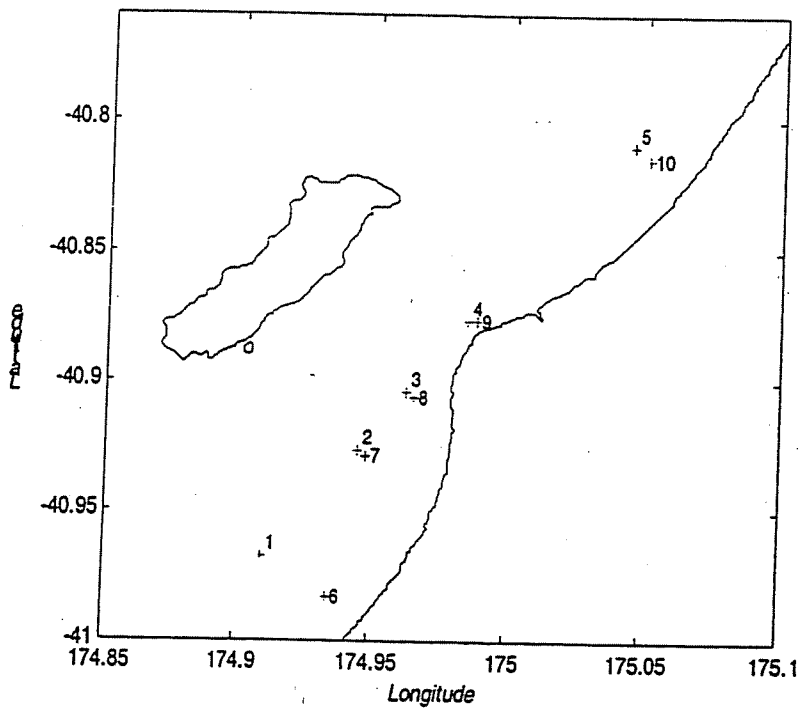

Figure 2.10: Local study area (inset of Figure 2.1) showing the 10 inshore sites along the Kapiti Coast for which wave conditions were estimated.

In these applications the model should be set up with the "offshore" boundary ($x = 0$) approximately normal to the incident wave direction (to within ±60° at most), so that waves can be accurately propagated between successive rows by stepping in the positive x direction. This requirement also reduces the area affected by propagation from the side boundaries, where the incident waves are not accurately specified. Further, the WBEND algorithm does not provide an accurate representation of the wave field "down-grid" of a land area. That is, if an island or headland occupies grid cells around (x_0, y_0), an unphysical "shadow" will affect wet cells with $x > x_0$ and $y \approx y_0$ (Figure 2.11). This is a separate effect from the genuine shadow produced in the down-wave direction from the obstacle, which the model can reproduce with reasonable accuracy in the area outside the "down-grid" shadow.

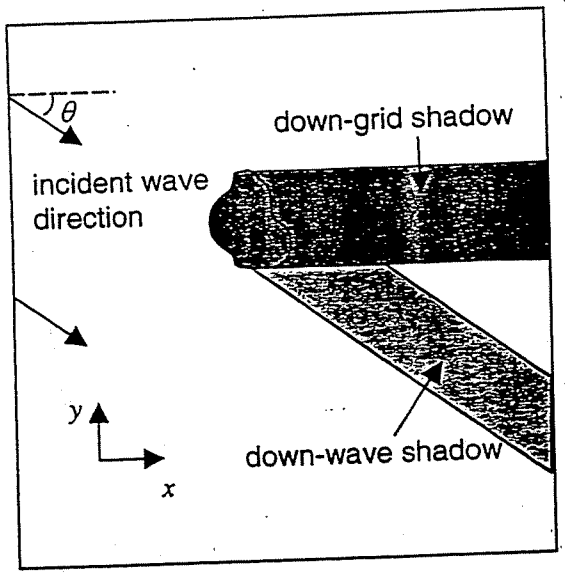

Figure 2.11: Schematic illustration of shadow effects in WBEND. Unphysical results are produced in the down-grid shadow of an island. The down-wave shadow is a genuine effect.

For these reasons, five separate model grids were used to ensure that, as far as possible, for each combination of offshore wave direction and output site there was at least one simulation that met both requirements. In any single model grid, a large area is affected by the "down-grid" shadow of Kapiti Island, but by re-aligning the grid, this shadow can be moved away from the site of interest.

The specifications of the various grids are listed in Table 2.1. Bathymetry for the region was assembled from the NIWA database of 10m contour levels, and interpolated onto the various rectangular model grids, each of which had a 250 m × 250 m cell size. Offshore wave conditions were specified as a time series of significant height, peak period and wave direction in deep water (> 100 m) off Kapiti Island. For each of the refraction grids, these parameters were applied at the offshore boundary, only running cases for which the incident wave direction was within ±60° of the grid's principle offshore direction. A monochromatic approximation was then used for the refraction model to derive wave height and direction at the inshore sites (listed in Table 2.2), with wave period taken as equal to the offshore value. The bed friction coefficient $C_f = 0.05$ was selected, and the eddy viscosity parameter was taken as $\varepsilon = 0.1\ m^2s^{-1}$. These values were found to provide a good reproduction of measured wave conditions in a similar modelling exercise in Pegasus Bay (South Island east coast), so were adopted for the present study in the absence of local inshore calibration data.

Swell penetration

It has already been indicated that swell from the Tasman Sea is expected to be considerably attenuated, and will have much less effect on the Kapiti Coast than

waves generated in the outer Cook Strait. Likewise, swell through Cook Strait will have little energy when it reaches this section of coast.

To quantify the effect of long-period waves, the WBEND model has been applied to several idealised cases of westerly and southerly swells with periods of 10 s and 12 s. Offshore wave heights of 1.5 m and 2 m were considered, approaching from 220°, 290° and 310°. Each of the 12 combinations of offshore height, direction and period was simulated. Distributions of swell height and direction are shown in Figures 2.12-14, for the simulations with 12 s period, 2 m offshore height.

For waves from 220° (Figure 2.12), grids aligned with the offshore boundary to the SW and W of Kapiti Island were used. Using the W grid, a "down-grid" shadow is evident to the east of Kapiti Island, having an unphysical influence on waves passing between the mainland and the southern end of the island. This simulation would therefore be unreliable at sites 4/8 and 5/10. In the SW grid simulation the incident wave direction is close to normal to the offshore boundary. This simulation appears not to be affected by Kapiti Island's down-grid shadow at any of the output sites. However the nearshore zone at Paekakariki, including site 6, is downgrid of Wairaka Pt on the mainland. As a result, the SW model underestimates wave height close inshore in this area, where the W grid provides a better simulation. Outside the shadow areas, the two simulations show similar results.

The W and NW grids were used for swells from 290° (Figure 2.13). In this case, the Waikanae River sites (4 & 9) are in the Kapiti Island down-grid shadow for both grids, so no reliable simulation could be obtained there. For swell from 310° (Figure 2.14), it becomes possible to use the N grid, so all sites are covered. Both these incident directions are near normal to the coast, so away from the effects of Kapiti Island, refraction produces only small changes in swell direction.

For southerly swells through Cook Strait, the window to Kapiti Island is quite narrow, and less than 15% of the energy will be captured. Note that 15% of the energy corresponds to 38% of the significant wave height. Thus, a 6-m southerly swell will result in about 2.0 m off Kapiti Island from a direction of 220°, and about 1.5 m at the 10-m isobath off Paekakariki and Raumati, approaching from about 260°. Further up the coast, north of Kapiti Island, a similar wave height may be expected from due west.

For waves from the southwest (240°) in the Tasman Sea, under similar assumptions for the directional distribution of the waves, about 6% of the energy could reach waters off Kapiti Island. Hence a 6-m southwesterly swell might produce 1.5 m offshore from the Kapiti Coast, approaching from 290°, 1.3 m at 10-m off Paekakariki and Raumati South, and 1.5 m at Peka Peka. Actual observations may be lower, as

these calculations have not included dissipation in the outer Cook Strait area which is likely to reduce the height further, closer to 1 m. Such swell is most likely to be accompanied by locally generated wind-waves.

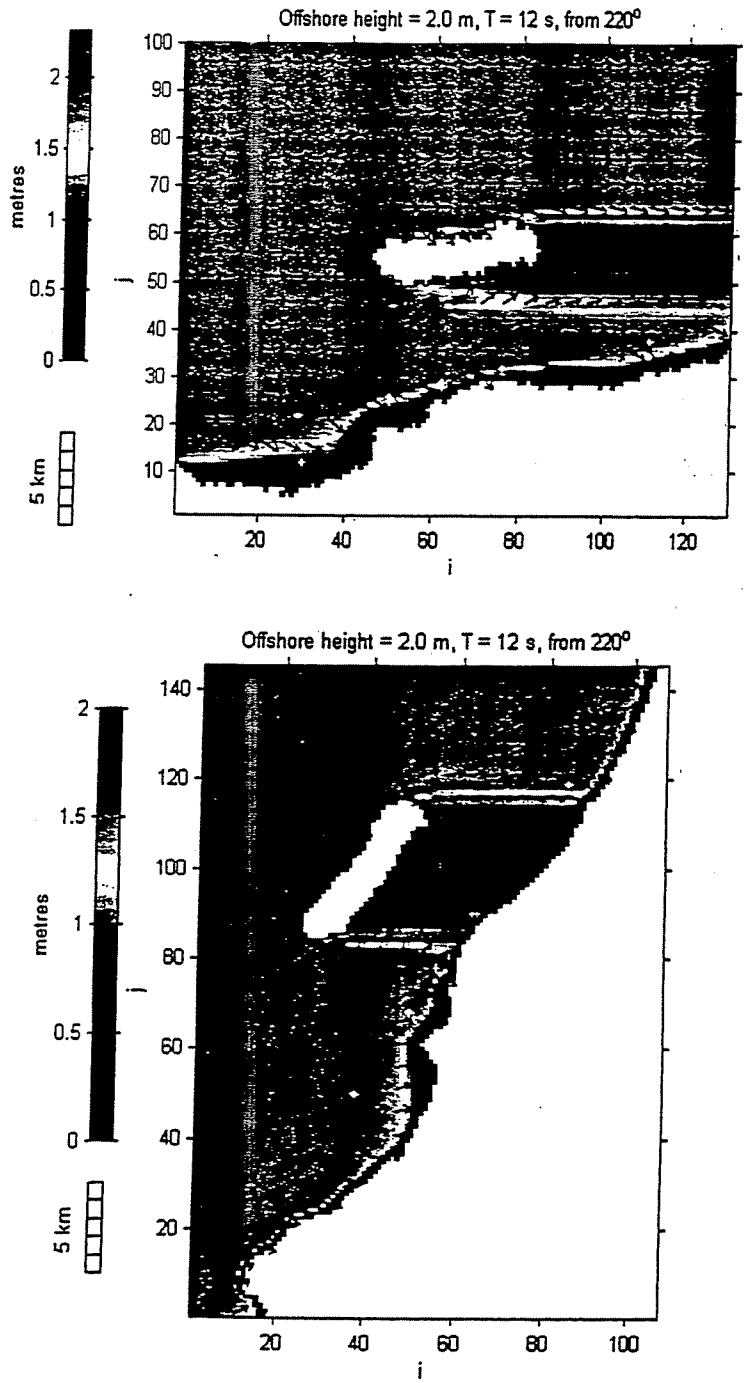

Figure 2.12: Refraction model simulation of swell with offshore height = 2.0 m, period = 12 s, direction = 220°, simulated on the SW grid (top panel) and on the W grid (bottom panel). The colour scale indicates wave height, and the arrows (in every 5th cell) show height and direction.

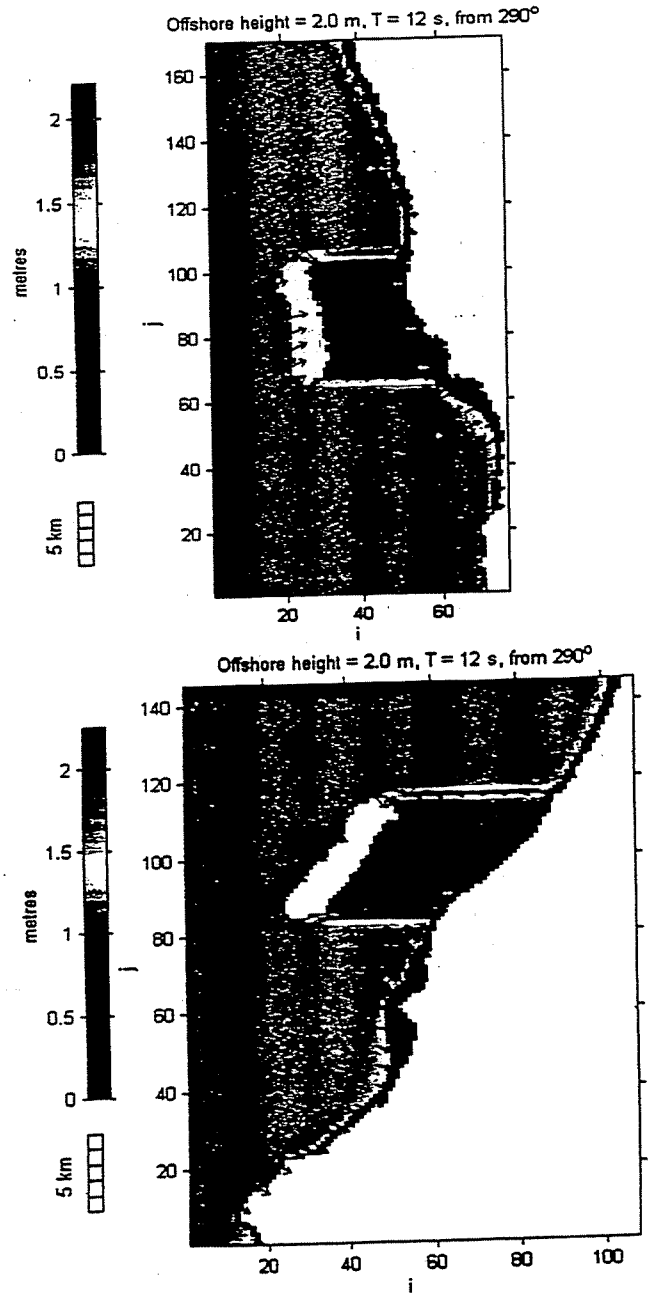

Figure 2.13: Refraction model simulation of swell with offshore height = 2.0 m, period = 12 s, direction = 290°, simulated on the W grid (top panel), and on the NW grid (bottom panel). The colour scale indicates wave height, and the arrows (in every 5th cell) show height and direction.

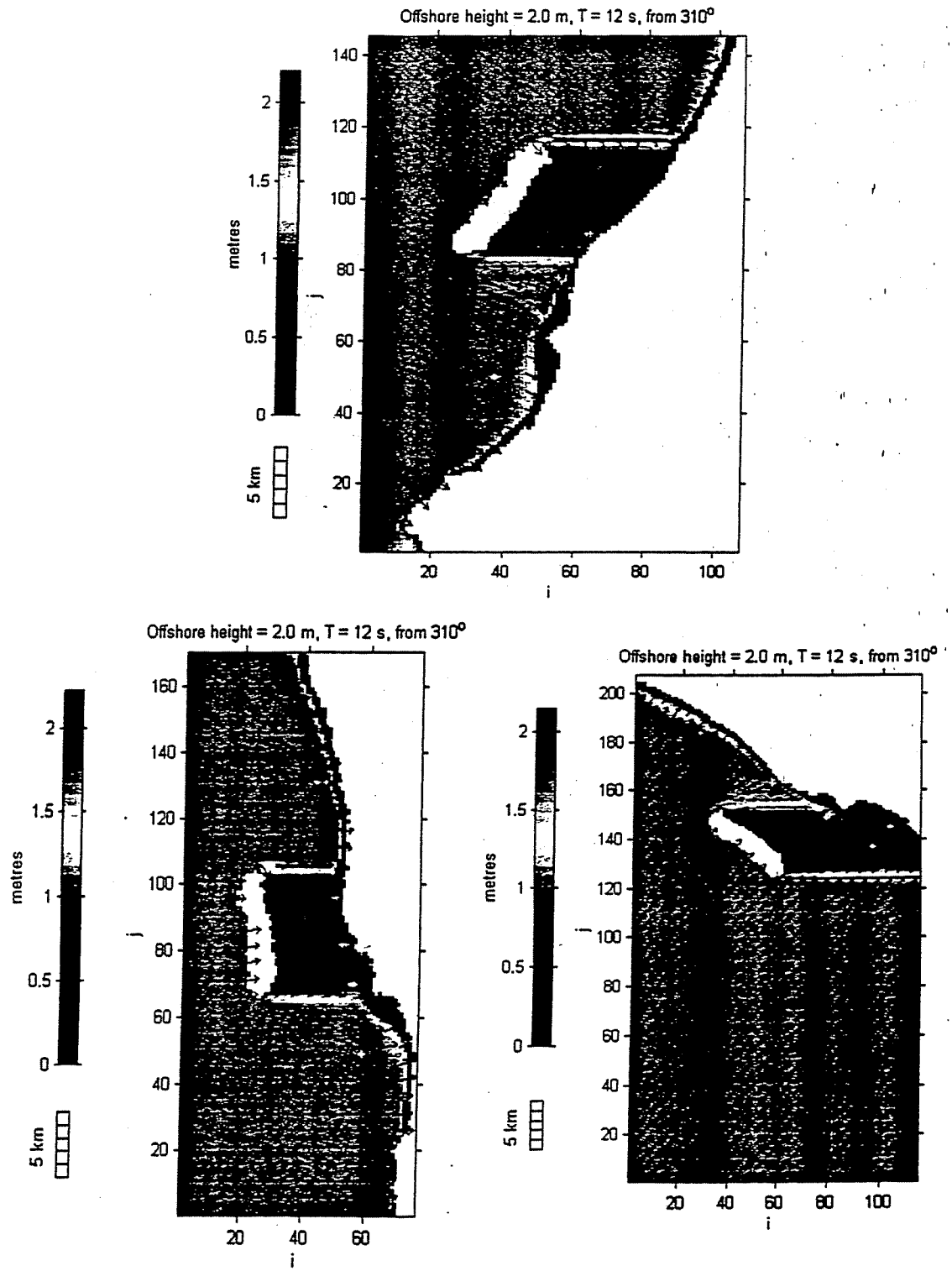

Figure 2.14: Refraction model simulation of swell with offshore height = 2.0 m, period = 12 s, direction = 310°, simulated on the W grid (top panel), the NW grid (bottom left panel) and the N grid (bottom right panel). The colour scale indicates wave height, and the arrows (in every 5th cell) show height and direction.

Refraction of synthesised waves

The refraction model was then applied using the offshore wave conditions computed for the waters off Kapiti Island as described in Section 2.7. This provides a synthetic record of wave height, period and direction that was applied to the offshore boundaries of the appropriate refraction model grids. After completing the separate runs, the results were merged. Where more than one run provided a valid result for a given inshore site, an average was taken over the valid runs (vector averaging was used for wave direction). There remained a limited number of events for which offshore data were provided but for which no valid inshore results could be obtained due to shadow effects. As noted above, when the offshore angle was between 270° and 300°, no valid hindcast could be obtained at sites 4 and 9 (see Table 2.2 and Figure 2.10), close to the middle of Kapiti Island's shadow.

The resulting time series of wave height and direction at each inshore site have been supplied electronically. The effects of refraction and shoaling vary from site to site. As an example, Figure 2.15 shows the refraction (change in direction) and shoaling (change in height) from deep water to a 20-m depth off Raumati South (site 2 of Table 2.2). Waves from the southwest through west are refracted moderately shoreward (to the right), with a slight loss of height due to the associated divergence of wave rays and some bed friction. At around 290° the wave incidence passes through shore-normal, and the directional shift changes sign. The effect of refraction becomes more pronounced for wave angles passing close to the southern end of Kapiti Island, the bearing to which (315°) provides a limiting value for waves reaching site 2 by this path. For offshore wave angles greater than 330°, we no longer used the W grid, and instead used the NE grid (not shown in Figures 2.12-14), in which only waves passing inside Kapiti Island from the north can reach site 2. The geometry of this path results in a band of directions around 360° at site 2, with relatively strong attenuation by spreading and friction. The sharpness of the jump at 330° is something of an artefact of simulating on different grids: in reality sea states with a mixture of waves passing both ends of Kapiti Island, as well as local generation within the Strait could be expected

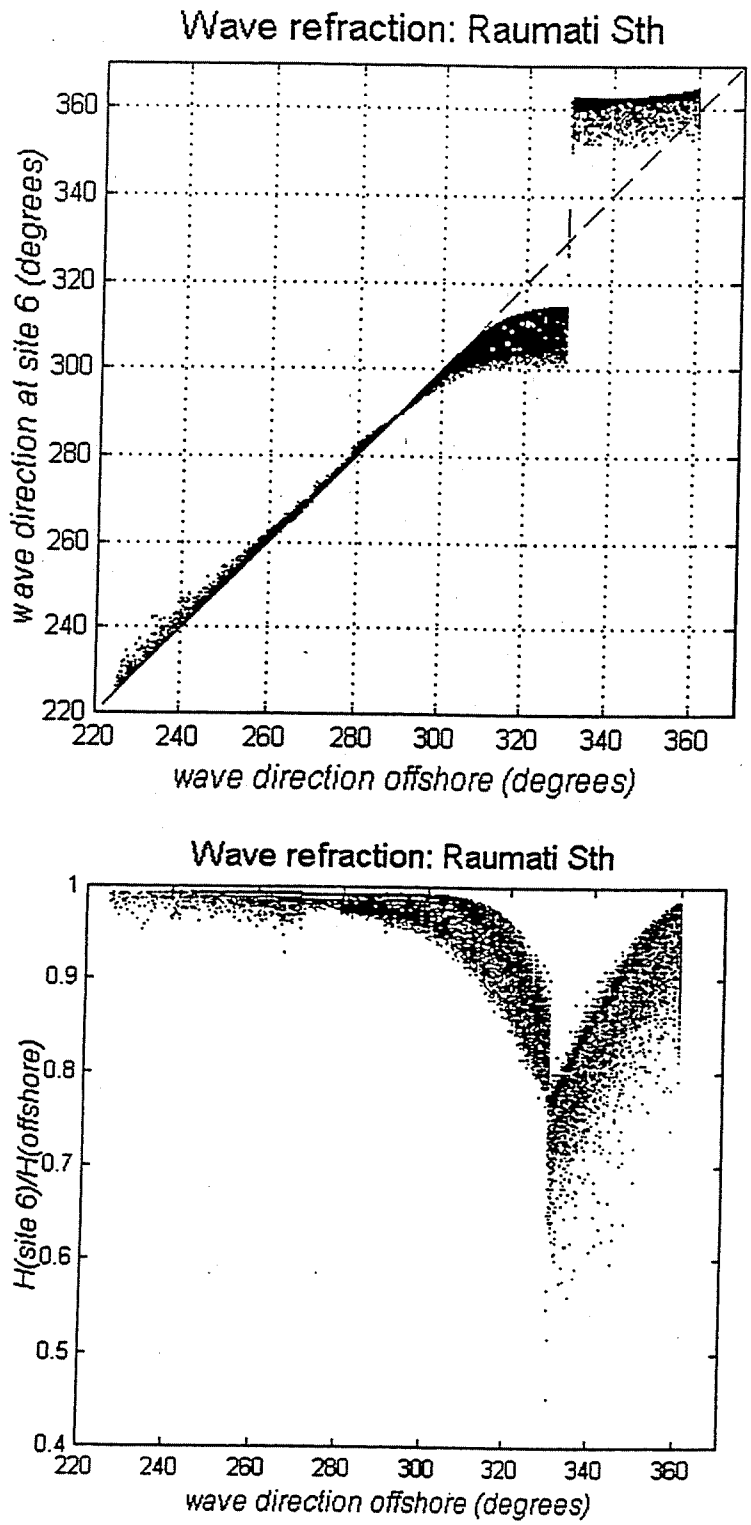

Figure 2.15: Refraction (upper) and shoaling (lower) from deep water to a 20-m deep site off Raumati South. The scatter diagrams show the inshore wave direction (in degrees) and ratio of inshore to offshore significant wave height, as a function of offshore wave direction.

Table 2.1: Model grids used in the Kapiti Coast refraction study. "Orientation" denotes the alignment of the principle offshore direction (negative *x*-axis).

	SW	W	NW	N	NE
cell size (m)	250	250	250	250	250
no. of cells	130 × 100	107 × 145	76 × 170	115 × 207	140 × 100
orientation	225°	270°	315°	0°	30°
origin: easting, northing (NZMG)	(2666030.09, 6012705.15)	(2636780.09, 6012705.15)	(2666030.09, 6012705.15)	(2636780.09, 6012705.15)	(2671780.09, 6012705.15)
origin: cell coords	(-19,1)	(-99,1)	(80,1)	(145,1)	(140,100)
bathymetry file	KAPCSTSW.MD	KAPCSTW.MD	KAPCSTNW.MD	KAPCSTN.MD	KAPNE2.MD

Table 2.2: Output sites for the Kapiti Coast refraction study.

site number	latitude (°)	longitude (°)	depth (m)	description
1	-40.968	174.910	20	Paekakariki
2	-40.927	174.945	20	South Raumati
3	-40.904	174.962	20	Paraparaumu - Marine Parade
4	-40.877	174.985	20	south of Waikanae R
5	-40.810	175.045	20	Peka Peka
6	-40.983	174.935	10	Paekakariki
7	-40.929	174.948	10	South Raumati
8	-40.906	174.965	10	Paraparaumu - Marine Parade
9	-40.877	174.988	10	south of Waikanae R
10	-40.815	175.051	10	Peka Peka

Validation

It is noted that the above analysis lacks local measurements to verify the approach. The measurements from further up the coast at Himitangi have value, but the complications of refraction and shadowing from Kapiti Island add potential sources of error. These may negate one another to leave quite reasonable estimates of the wave conditions, but they also may compound. The uncertainty can only be dispelled by conducting a measurement campaign to establish the wave conditions at a nearshore site under a range of wind events. These measurements should be directional, so that the alongshore component of the wave energy can be determined, and should be made in water depths sufficiently shallow so that the measurements indicate what is actually happening at the coast. An S4 current meter at a depth of 10m is recommended.

3. STORM SURGE AND TIDES

3.1 Background

Storm surge is normally defined as the temporary elevation of sea level, above the predicted tide level, by a varying combination of:

- low barometric pressure that is compensated by a regional rise in sea level (called "inverted barometer" or IB), and;

- adverse winds that cause seawater to "pile up" along the coast. Such adverse winds for Kapiti usually come from alongshore winds that blow from the north and north-east (causing a set-up of the sea to the left by the centrifugal force of the Earth's rotation) and onshore winds blowing from the north-west. Conversely, southerly and south-westerly winds are unlikely, acting alone, to cause high set-up in sea level along the Kapiti coast.

At the shoreline and foredune, a further elevation in sea level arises from wave set-up in the surf zone (non-linear effect) and subsequent wave run-up (swash zone). These wave-derived set-ups are dealt with separately from storm surge.

The critical aspect for coastal hazard assessment is not just how big the storm surge set-up is, but how big the high tide is likely to be. When the tide range is low during neap tides (first and third quarters of the Moon's phase), a storm surge event is unlikely to create major problems. But a moderate storm surge coinciding with a high spring or perigean tide, creates a high risk of impact and damage occurring. Furthermore, high tide level is entirely predictable e.g., the next 100 years, based on the known movement of the Earth and Moon relative to the Sun.

Longer term elevation in sea level at seasonal and year-to-year timescales is also an important "background" contributor to storm surge levels. In particular, higher than normal sea levels occur in late summer (due to thermal expansion of seawater) and also during La Niña episodes of 2–4 year duration. The contribution from these sources will seldom exceed 0.15 m above predicted tides.

It is important to appreciate that the occurrence of a storm surge doesn't necessarily imply severe coastal erosion. The latter depends greatly on the approach angle of waves to the coast, wave period (e.g., wind waves or swell) and the tide level.

This chapter presents results on previous storm-surge events along the Kapiti coast based on a combination of recorded sea-level data (NIWA gauge at Kapiti Island), analyses of long-term barometric pressure and wind data (Paraparaumu Airport) and

synopsis of historic storm events. From these analyses, an upper bound on storm surge set-up for next 50–100 years is estimated.

3.2 Tides and Storm Surge (Kapiti Island Sea-level Gauge)

NIWA co-ordinates a network of 11 open-coast sea-level gauges around New Zealand. One of these sites is located on Kapiti Island. The gauge has only been operational since July 1997, providing 3 years of data. While this record is short, we can establish an approximate link between storm surge and the relative contributions of barometric pressure and winds. By this means, we can utilise longer climate records to extend the database. The 3 years of data also provides a good basis for predicting tides over the next 100 years.

Tides

There is considerable spatial variation in tides along the Kapiti Coast, especially the lunar semidiurnal (twice-daily) tides (M_2 and N_2), as shown in Figure 3.1 and Table 3.1. The data are from a tidal model of NZ's entire Exclusive Economic Zone (Walters et al., 2000). In Figure 3.1 the numbers along the coast correspond to the node numbers in the model and in Table 3.1 the distance is calculated from the distance between nodes, starting at Wairaka Point in Pukerua Bay. The Table shows that the main lunar M_2 tide increases in amplitude by ~320 mm in 41 km along the Kapiti Coast and the N_2 tide (due to the Moon's elliptical orbit around the earth) more than doubles up the coast, increasing by 65 mm. The reason for this behaviour is that the Kapiti Coast is within the influence of Cook Strait where tidal patterns are extremely complex. For both tides, M_2 and N_2, there is a phase difference of nearly 180° through the strait (meaning that high tide on one side coincides with low tide on the other) and at Makara the tides almost completely cancel each other out (called an "amphidrome"), producing near zero tide range. The solar twice-daily tide S_2 also decreases in amplitude as Cook Strait is approached, with the Kapiti Coast being just south of a region of resonance of these tides between the South Taranaki Bight and Tasman and Golden Bays.

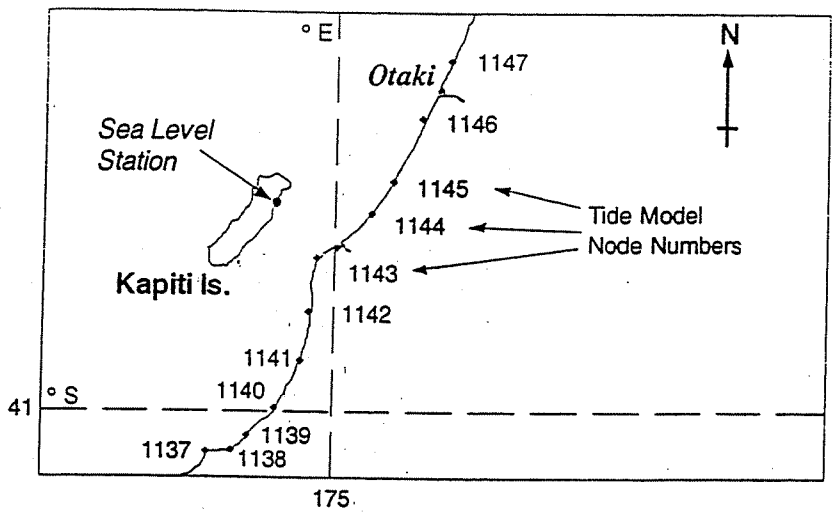

Figure 3.1: Location of tide-model grid points along the Kapiti coast (for Table 3.1) and the NIWA sea-level station on Kapiti Island.

Table 3.1: The change in half-range amplitude (mm) of the 3 dominant twice-daily tides (M_2, S_2, N_2) along the Kapiti coast (from south to north) predicted by the tidal model. These are used to determine mean high water spring (MHWS) and a high astronomical tide (HAT), that is only exceeded ~1% of high waters, relative to the mean level of the sea. Node #1143 corresponds to Paraparaumu Beach. [Note: HAT is defined here as the combined sum of all 3 main tidal constituents coinciding together i.e. a perigean-spring tide.]

Model Node No.	Latitude (°N)	Longitude (°E)	Distance north (km)	M_2 (mm)	S_2 (mm)	N_2 (mm)	MHWS (mm)	HAT (mm)
1137	-41.0306	174.8700	0.0	395	229	55	624	679
1138	-41.0297	174.8956	2.1	413	235	60	647	707
1139	-41.0178	174.9124	4.1	428	239	63	667	730
1140	-40.9974	174.9405	7.3	451	245	68	695	764
1141	-40.9614	174.9659	11.9	486	254	76	739	815
1142	-40.9242	174.9734	16.0	527	265	85	792	877
1143	-40.8844	174.9816	20.5	594	282	99	876	974
1144	-40.8512	175.0355	26.4	644	294	108	938	1047
1145	-40.8277	175.0578	29.6	662	298	112	960	1072
1146	-40.7801	175.0861	35.4	690	304	117	994	1111
1147	-40.7356	175.1135	40.8	714	310	121	1024	1145

The implication of the considerable spatial variation of tides along the coast is that estimates of extreme tides made using data from the sea-level recorder on Kapiti Island need to be scaled to obtain the corresponding statistics along the coast. There are numerous ways of doing this, but the preferred one is to use MHWS (mean high water springs) in Table3.1. MHWS, calculated by adding the lunar M_2 and solar S_2 amplitudes (half-range), represents the tide level above the mean level of the sea that is exceeded by ~10% of the time by tides. MHWS for the sea level recorder is 911 mm. This corresponds to a position between nodes 1143 and 1144 on the coast, directly east of the recorder. Thus, extreme tides to the north (Otaki Beach) need to be scaled up by as much as 112% and those to the south (Pukerua Bay) need to be scaled down by as little as 68%.

The tidal amplitudes from the model are somewhat higher than those measured at Kapiti Island (609 mm compared with the measured value of 548 mm for M_2). The reason for this is that the present model has a grid that is too coarse in the Cook Strait region, where the tide range changes rapidly. Work is underway to improve the model grid, but in the meantime the data from the present model can be used with confidence in a relative way, i.e., to compare tides from one location to another.

The effect of Cook Strait on tides is profound. The effect of Cook Strait on storm surge is completely unknown. Similarly, the spatial variation in storm surge along the Kapiti Coast is unknown. Currently, research is underway to identify the variation in storm surge around the country, but no results are available yet. Work by Goring (1995) on 15 sea level records around the country relating barometric pressure to storm surge showed that west coast sites generally experience higher storm surge than east coast sites and that barometric pressure changes generally precede storm surge (whereas on the east coast, storm surge often leads barometric pressure).

The procedure of Goring (1995) was applied to the data from the Kapiti Island recorder from 24-Jul-1997 to 28-Jul-2000 (1100 days), resulting in an optimum barometric factor of –0.530 and a regression coefficient of 0.371, with sea level leading pressure changes on average by 3 hours. The interpretation of these quantities is that sea level responds to changes in barometric pressure with an average 0.53 cm rise in sea level for every hPa of fall in pressure and vice versa, and 37% of the variation in sea level (excluding tides) can be explained by barometric pressure. These results differ from those of Goring (1995) for west-coast sites, but the record from Kapiti Island is only 3 years duration and in that time there were few large storm-surge events. Also, these results are for the entire ensemble of data, not for individual events.

Examination of the sea-level record in Figure 3.2 indicates that for most large barometric pressure events, both positive and negative, sea level appears to correspond quite closely to inverted barometer. However, in between events, there are considerable differences between the inverted barometer record and the sea level record and it is these periods that govern the evaluation of barometric factor to a large extent. For the larger events, there is no evidence of amplification of inverted barometer, as was found for other west-coast sites by Goring (1995). Therefore, for the purpose of design, in using barometric pressure as a surrogate for sea level, a conservative strategy is to use the inverted barometer, i.e. a barometric factor of −1 cm/hPa.

The largest measured storm surges at Kapiti Island in the 3-year period were ~0.27 m above predicted tides on 8 November1997 and 1 June 2000. These occurred during NW to NNW winds up to 14 ms^{-1} (28 knots) generated by low-pressure systems with central pressures of 989 hPa to 992 hPa. In both cases, the storm surge was close to the inverted barometer value, which confirms the above strategy of using a factor of −1 cm/hPa. This result also suggests that storm surges in the Kapiti area, at least over the past 3 years, were mainly caused by low barometric pressure, with a smaller contribution from wind set-up. However it is important to consider that the sea level recorder is on the east (i.e., leeward) side of Kapiti Island, so onshore or alongshore winds piling water up on the west side may actually cause depressed water levels where the recorder is.

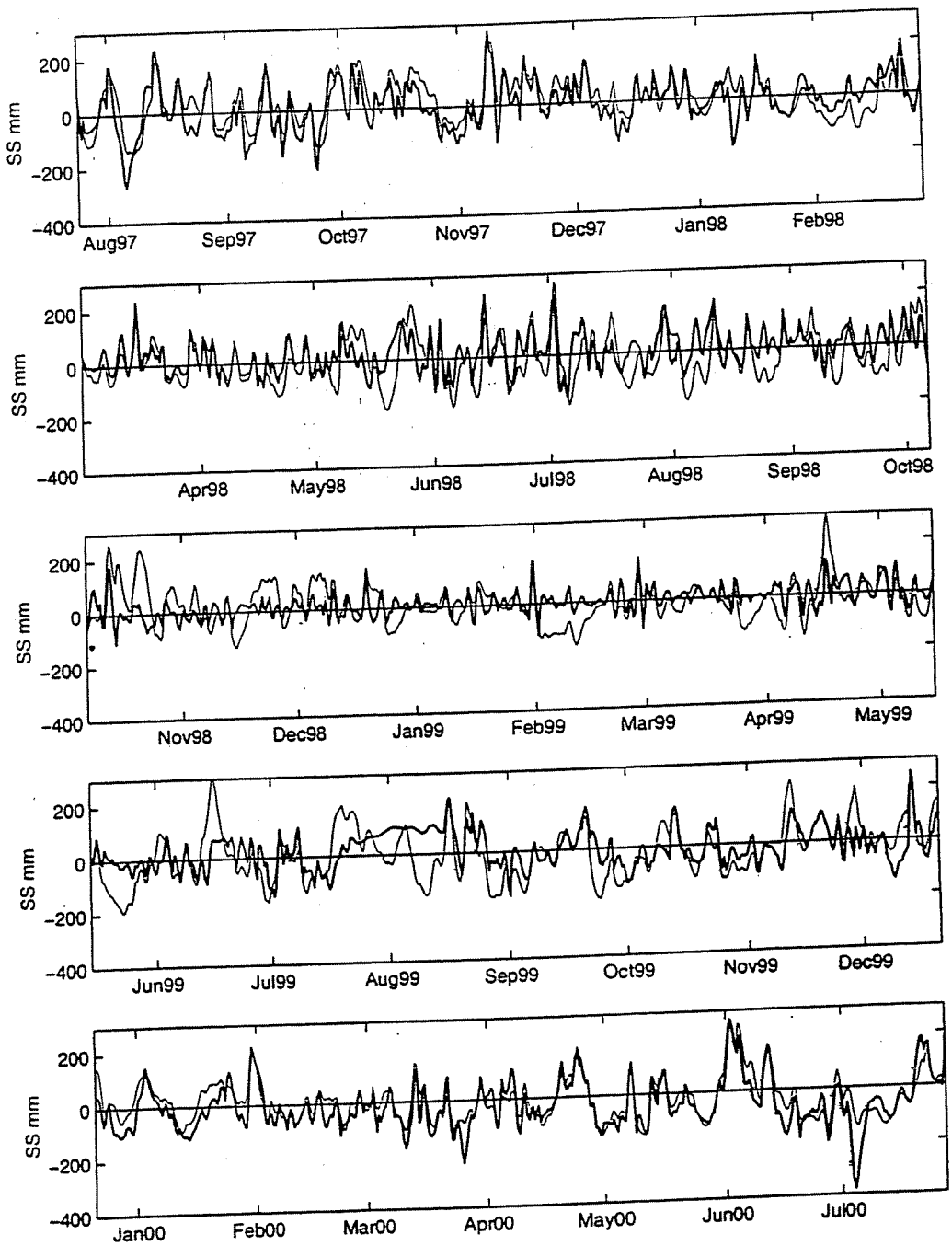

Fig. 3.2: Storm surge (heavy line) and inverted barometer (thin line) recorded by the Kapiti Island sea-level recorder from 24-Jul-1997 to 26-Jul-2000. Negative values mean a set-down in sea level below the predicted tide. [Note: a gap occurred over the period 21 July to 15 August 1999.]

3.3 Extreme Tides

Over 60 tidal constituents (e.g., M_2, S_2) were isolated from the 3-year tidal record from Kapiti Island. These tidal constituents don't vary much, being a function of the stable relative motions of the moon, earth and sun, so 3 years is sufficient to isolate all

but the long-term lunar node tide, which although quite small, is accounted for by the prediction package (Foreman, 1977). This information was used to predict high-water tide levels over the 100-year period from July 1997 (start of the Kapiti record) to July 2097. The predicted tides also include an average annual (seasonal) cycle of 0.036 m amplitude. The frequency distribution of predicted high water levels over the 100 years is shown in Figure 3.3. A closer view of the predicted extreme high water levels is given in Figure 3.4. An example listing of dates for which high water will be at least 1.09 m is given in Table 3.2. The highest tide in the 100-year period will be nearly 1.11 m above MLOS in March 2082.

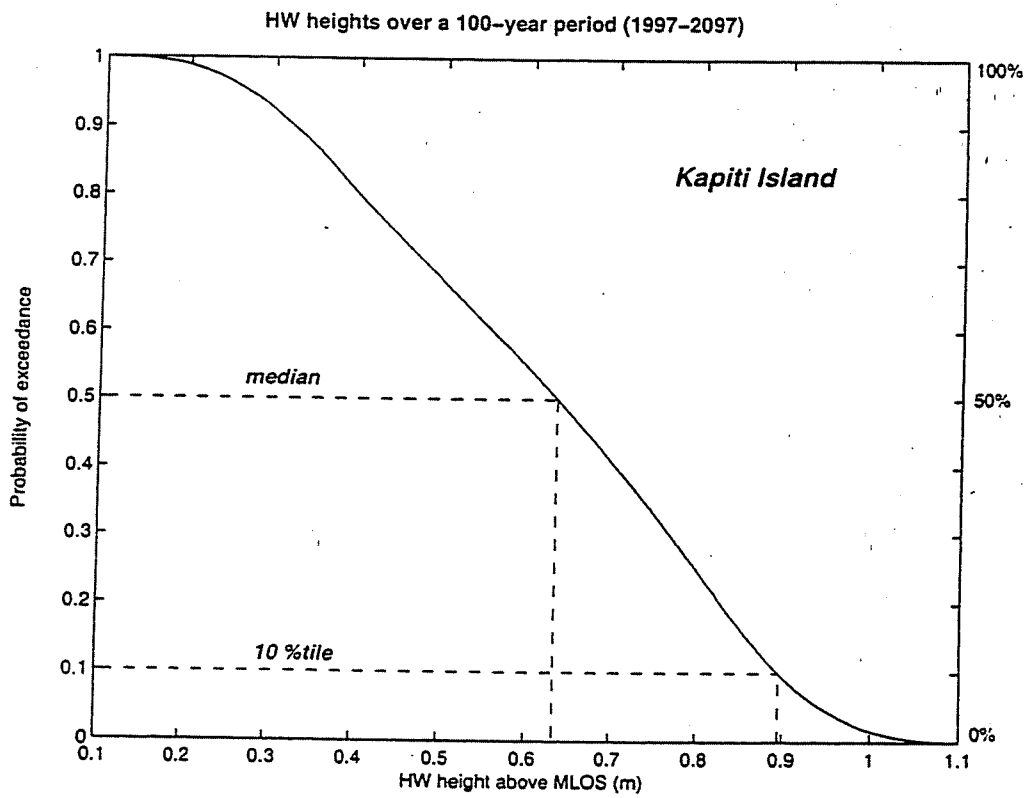

Figure 3.3: Probability of exceedance curve for all predicted high water (HW) levels at Kapiti Island for the 100-year period July 1997 to July 2097. The high tide levels are relative to the mean level of the sea (MLOS). The 10-percentile exceedance probability is approximately the same as MHWS.

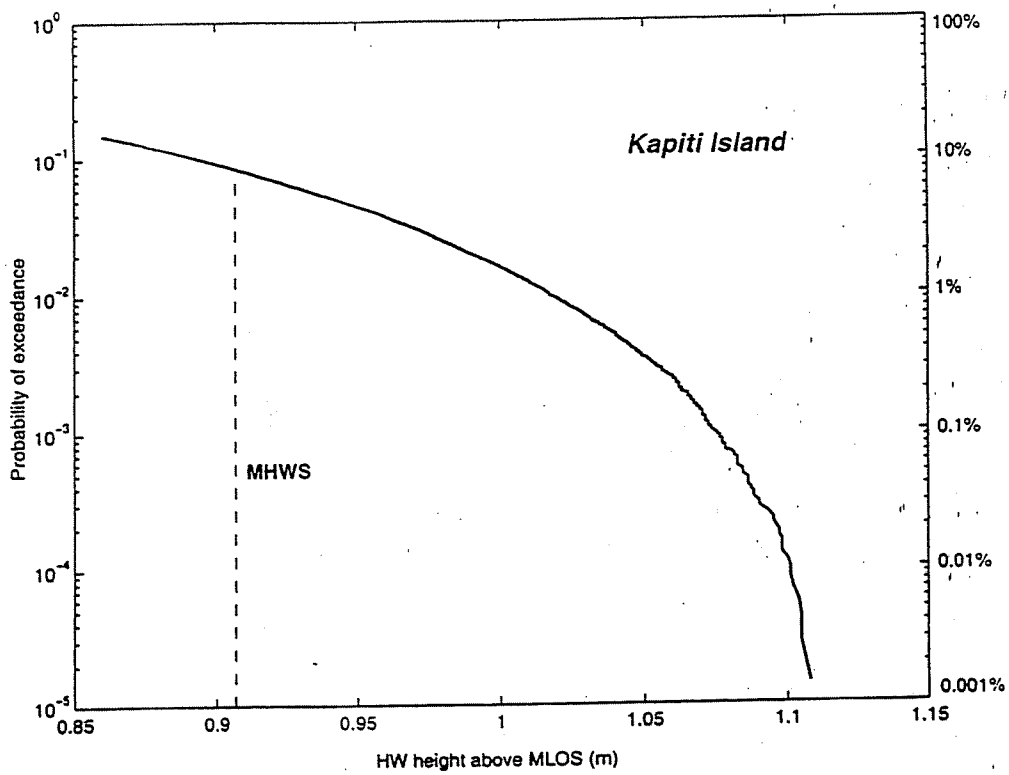

Figure 3.4: Probability of exceedance curve for extreme predicted high water levels at Kapiti Island for the 100-year period July 1997 to July 2097. The high tide levels are relative to the mean level of the sea (MLOS). The MHWS level (exceeded by ~10% of high waters) is marked for comparison.

Table 3.2: Dates for the most extreme high tides (≥1.09 m above the MLOS) over the 100 years.

Date	HW (m)	Date	HW (m)	Date	HW (m)
30-Mar-2002	1.10	02-Mar-2029	1.10	02-Apr-2056	1.10
20-Mar-2003	1.10	22-Mar-2038	1.10	05-Mar-2064	1.11
20-Feb-2011	1.10	23-Mar-2038	1.10	25-Mar-2073	1.11
21-Mar-2011	1.09	23-Mar-2042	1.09	13-Apr-2074	1.10
11-Mar-2020	1.10	23-Feb-2046	1.09	16-Mar-2082	1.11
09-Apr-2020	1.10	15-Mar-2055	1.10	07-Mar-2091	1.09
30-Mar-2021	1.10	01-Apr-2056	1.09	05-Apr-2091	1.10

The extreme tides at or above MHWS are important because if even a small storm event occurs on these "red alert" days, which can be predicted well in advance, there will be a high risk of inundation of the coastal dunes and seawalls. Extreme tides to the north (Otaki Beach) need to be scaled up by as much as 112% and those to the south (Pukerua Bay) need to be scaled down by as little as 68%.

3.4 Barometric pressure (Paraparaumu)

The sea-level record from Kapiti Island is too short to estimate return periods of storm surge. However barometric pressure records are available for the 38-year period since January 1962 from Paraparaumu Airport. Of most interest is the minimum mean sea level pressure (MSLP) distribution, as most of the large storm-surge events have common elements—low barometric pressure, high tides and adverse winds. Figure 3.5 shows the minimum daily barometric pressure (MSLP) for the Paraparaumu record, which illustrates the episodic nature of the low-pressure "spikes". Three well known events in recent time are marked with asterisks, being Cyclone *Giselle* (the so-called Wahine storm) in April 1968, the storm of September 1976 which caused severe erosion along the Kapiti coast, and the more recent event on 17 April 1999 (the lowest recorded pressure spanning the 3-year sea-level record).

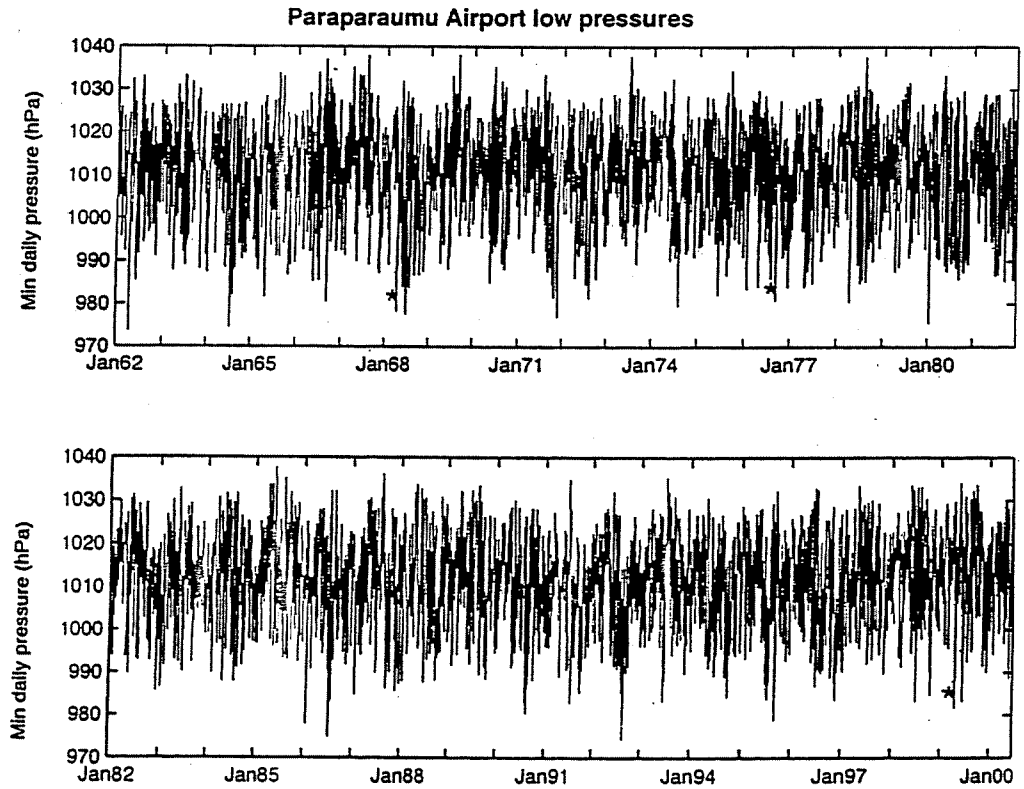

Figure 3.5: Minimum daily MSLP for Paraparaumu Airport from January 1962 to June 2000, based on hourly measurements. Note: barometric pressure is measured in hecto-pascals (hPa), which is the equivalent of millibars (mb).

Of most relevance to storm surge levels is the frequency of deep low-pressure systems passing through the region. The minimum daily pressures were sorted in ascending order and the lowest values plotted as a frequency (probability) plot (Figure 3.6). The 1968 and 1976 events are marked. Interestingly, the barometric pressure of 980.8 hPa wasn't excessively low during the devastating 1976 storm. This low pressure was

surpassed by 19 other lower events during the 38-year period. This illustrates the whole issue of joint occurrence and probability of several "components" combining together when attempting to derive return periods of various storm surge levels and then including the wave set-up and run-up.

The lowest pressure recorded was 973.6 hPa on 15 April 1962, yielding an equivalent sea-level set-up (inverted barometer) of just over 0.4 m due to the low pressure alone.

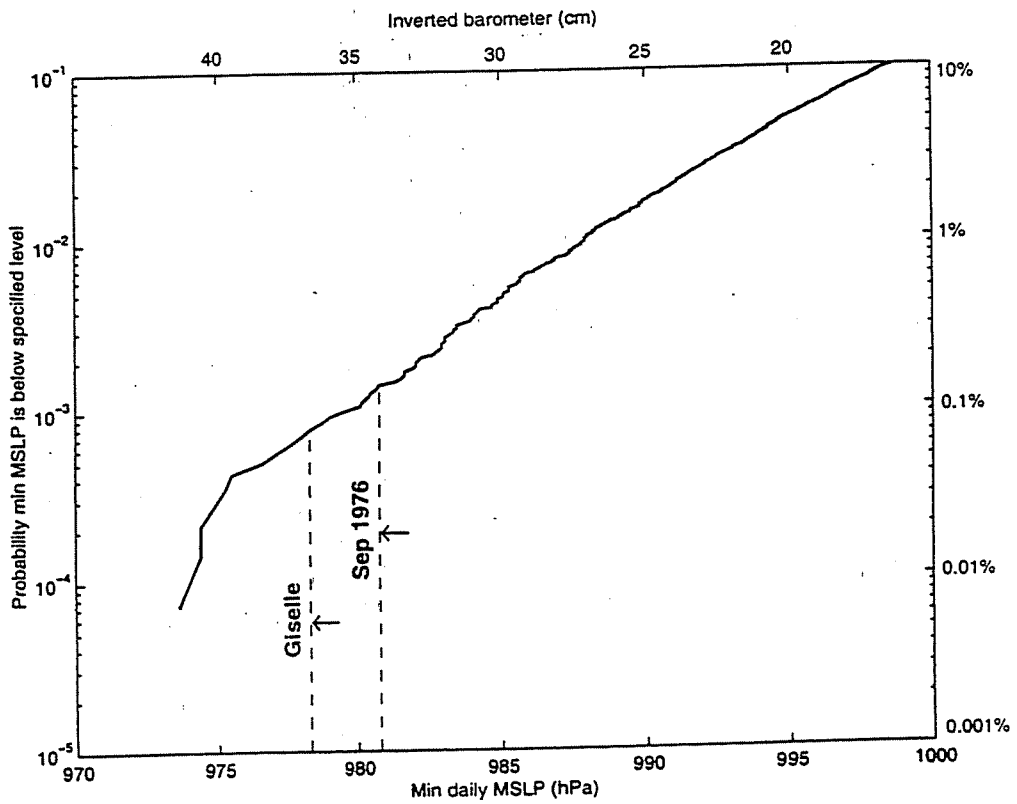

Figure 3.6: Frequency distribution of minimum daily MSLP for Paraparaumu Airport from January 1962 to June 2000, based on hourly measurements. The right axis gives the % of days in the 38-year period that pressures were lower than a selected MSLP. The top axis converts the MSLP into an equivalent elevation in sea level (cm) due to the inverted-barometer effect.

3.5 Historic Storm Events

Recorded observations of historic storms along the Kapiti coast are patchy. Two historic events in the 1950s caused severe erosion along the coastline from Paekakariki and Raumati (Donnelly, 1959). No climate data is available for this period, but newspaper articles and observations provide some indications:

- 9–11 July 1954 event—minimum low pressure of around 990 hPa with north-west winds, followed by a southerly gale that gusted to nearly 90 knots at Rongotai

Airport. Tide ranges were low (neap), with the predicted high tide at Kapiti Island only reaching 0.4 m above MLOS. It appears that the storm-surge component was probably small to moderate, coinciding with neap tides and therefore the erosion was largely the result of wave action.

- 12–13 October 1957—minimum low pressure of 988 hPa (inverted barometer set-up of 0.27 m) accompanied by gale-force north-west winds (gusts up to 57 knots recorded at Kelburn). Tide ranges were high (spring), with the predicted high tide at Kapiti Island reaching 0.9 m above MLOS. The *Evening Post* reported that on Sunday morning (13 October, 1957), "heavy seas pounded a mile of Paekakariki Beach, cutting several feet into the sandhill". Further, "all residents could do at the height of the gale at midday was to watch the waves, estimated to be 20 to 30 feet (6–9 m), slash their way through flimsy protective walls." Obviously, the damage was mainly due to wave run-up, but was supported by a spring tide that peaked soon after midday and a moderate storm surge (estimated to be 0.4–0.5 m from IB and wind set-up), elevating the local sea level and exposing the toe of the foredune.

Two other major events occurred in April 1968 (Cyclone *Giselle*), with no known accounts of erosion, and the September 1976 storm (Gibb, 1978; that caused severe erosion:

- 10 April 1968—although this event isn't documented as causing erosion, it is highlighted because the minimum pressure reached 978 hPa and was accompanied by a short 8-hour period of gale-force SSW winds (210°) on the Kapiti coast. At Paraparaumu Airport, the average 10-minute wind speed reached 60 knots. The inverted-barometer set-up alone would have been ~0.37 m, however an alongshore wind from the south will tend to cause set-down at the coast. Therefore the set-up in sea level along the Kapiti coast was likely to have been no more than 0.4 m, and combined with only a mean tide at the time (high water 0.4–0.5 m above MLOS), provides an explanation perhaps for why there are few known reports of storm damage.

- 11–13 September 1976—minimum pressure at Paraparaumu reached 981 hPa on 13 September, hovering at very low pressures below 987 hPa for two days on 12–13 September. The situation as set up by a slow-moving depression (970 hPa) west of Taranaki (Gibb, 1978). The equivalent inverted-barometer set-up would have been sustained at approximately 0.30–0.35 m over both days. The local winds at Paraparaumu Airport reached 34 knots (10-minute average) from NNW (330°), while out at sea in the South Taranaki Bight, ships recorded 50-knot NW winds and 11–13 m swells (Gibb, 1978). The wind-stress surge component would have been approximately 0.25 m. From beach surveys, Gibb (1978) concluded that the total storm surge set-up was 0.72 m above the predicted spring-tide high

waters for the two days of 0.75 m above the MLOS. This means the total sea elevation at high water (excluding wave run-up) would have been nearly 1.5 m above the MLOS (or 1.65 m above the geodetic MSL datum (Wellington Datum 1953).[1] Gibb (1978) also deduced from the driftwood line that the wave run-up reached a vertical elevation of 2.6 m higher than the normal driftwood line.

4. SEA-LEVEL VARIABILITY AND TRENDS

4.1 Sea-level variability

"Mean Sea Level" is somewhat of a misnomer, as it is often thought of in terms of a "datum", implying that sea level is constant. Sea-level variations at seasonal, interannual (year-to-year) and decadal timescales have an important role in determining the "background" sea level present in any given month. If the "background" sea level is elevated, it will exacerbate storm surges and tides that operate at hourly and daily timescales. Recent research has improved our understanding of seasonal, interannual (year-to-year) and decadal variability in sea level around New Zealand (e.g., Bell and Goring, 1997; Bell et al., 2000). But progress has been severely hampered by the lack of any long-term open-coast sea-level gauges, and the Kapiti coast is no exception. Some seasonal data is available from the 3-year Kapiti Island gauge and interannual variability was gleaned from Port of Taranaki tide-gauge data (1986–1998). Long-term sea-level change was determined from Auckland and Wellington ports.

Seasonal or annual cycle

Generally, the annual cycle in sea level is small around New Zealand and Kapiti is no exception. The mean variation from the 3-year Kapiti Island gauge is just under ±0.04 m, peaking in February. The increase in summer occurs due to the thermal expansion from warmer seawater. The annual cycle is included in the prediction of high-water levels discussed in Section 3.3.

Interannual variability

The year-to-year variation in sea level is greater than the seasonal cycle. It is intricately connected with the El Niño–Southern Oscillation (ENSO) system. Figure 4.1 shows a comparison with sea levels at both Taranaki (west coast) and Moturiki (east coast) and the Southern Oscillation Index or SOI. Sea level at both sites tracks

[1] Based on the present mean level of the sea (MLOS) being 0.16 m higher than the geodetic MSL Datum (1953) at the Port of Wellington. Figure kindly supplied by John Marks (Wellington Regional Council).

closely with the SOI. Therefore around the North Island, sea level is elevated above normal during La Niña episodes (e.g., 1989 and 1998–99). Conversely, El Niño episodes tend to supress sea level lower than normal. The range at Taranaki for the filtered (long-term) variability is ±0.1 m and by inference applies along the Kapiti coast. Taking into account longer records from elsewhere in New Zealand, the interannual elevation of background sea level at Kapiti could be up to 0.15 m for a few months during strong La Niña episodes (Bell et al., 2000).

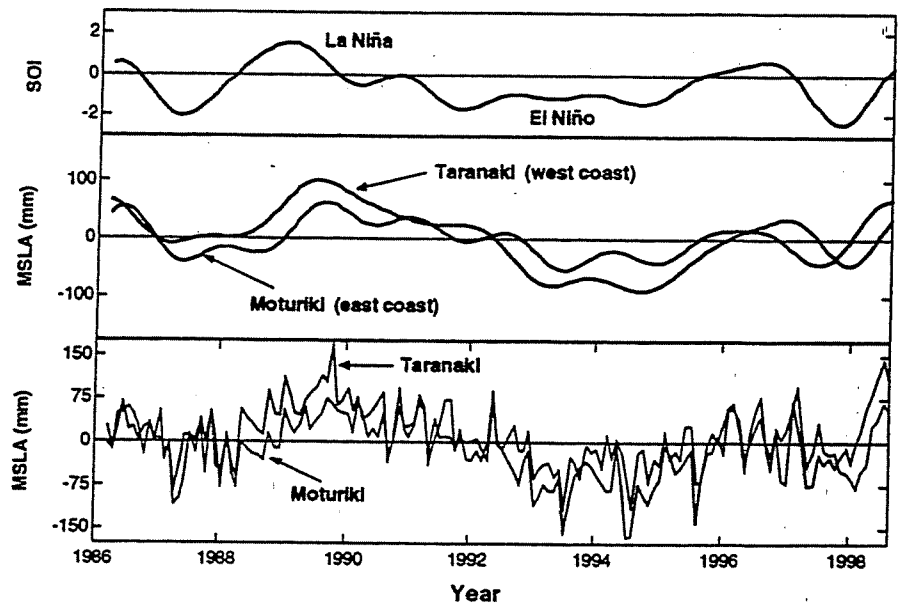

Figure 4.1: Monthly-mean sea level anomaly (MSLA) for Port of Taranaki (blue) and Moturiki (Mt Maunganui) on the east coast for 1986–1998. The bottom panel shows the actual monthly means, the middle panel is filtered to remove short-term fluctuations and the top panel shows the SOI, with positive values indicating a La Niña.

4.2 Sea-level trend

The trend in sea-level rise for the last 100–150 years is small, with a global mean of +1.8 mm/yr. However, over a century, this equates to an increase of 0.18 m. This ongoing rise in sea level gradually increases the probability of exceedance of any specified hazard datum (relative to the landmass) from coastal inundation events. Therefore sea-level rise should be factored into any long-term coastal plans.

Historic change

An analysis by Hannah (1990) of sea-level trends from 1900–1988 from tide-gauge data at New Zealand's four main ports (Auckland, Wellington, Lyttelton, Dunedin) produced a national average rise in sea level of +1.7 mm/yr (range=1.3–2.3 mm/yr). This is similar to the global average of +1.8 mm/yr. The two North island ports exhibited rates of 1.3 mm/yr (Auckland) and 1.7 mm/yr (Wellington). So far there has been no apparent acceleration in the rate of rise (Bell et al., 2000).

With respect to the past century, the 0.1–0.25 m rise (average=0.18 m) in global mean sea level has been due largely to a concurrent increase in global temperatures since the end of the Little Ice Age (*c.* 1800). This has been forced mainly by increases in solar input and a small warming effect due to ozone depletion in the stratosphere (Nunn, 1998). The climate-related factors contributing to this rise include thermal expansion of the ocean and melting of glaciers, small ice caps and to a lesser extent, the large Greenland and Antarctic ice sheets.

An in-depth analysis by Bell et al. (2000) of the Auckland sea-level data has shown that medium-term variability at 20–30 year cycles (called the Interdecadal Pacific Oscillation) has a significant effect on the trend i.e. it is not a steady rise. For instance, since a climate regime shift in the mid 1970s, the trend in sea level at Auckland over the past 25 years has been almost static. This was caused by a "flow-on" effect from the unusually persistent El Niño behaviour since 1976, which tended to suppress regional sea levels lower than normal. This effect also occurred at Taranaki (Figure 4.1) and by inference Kapiti. The next few years should see another climate regime shift of the interdecadal phase resulting in more frequent La Niña episodes. Consequently, regional sea levels are expected to rise more rapidly over the next decade, similar to the 1950s, and "catch up" to the going rate this past century of +1.7 mm/yr.

Projected sea-level rise

Projections of future sea-level rise, within the context of climate change, are regularly addressed by the Intergovernmental Panel on Climate Change (IPCC). The IPCC was established in 1988 by the World Meteorological Organisation (WMO) and the United Nations Environment Programme (UNEP). The IPCC is charged with assessing the most up to date scientific, technical and socio-economic research in climate change, including sea-level rise. They produced major assessment reports in 1990 and 1995, and the Third Assessment Report is scheduled for completion in March 2001. The 1995 Report contains model projections for increases in global sea level for various "greenhouse" gas (e.g., CO_2) emission scenarios and climate factors (Warwick et al., 1996).

Projected sea-level rises for three different greenhouse gas emission scenarios in combination with climate factors that cover the mid-range and upper and lower limits are listed in Table 4.1. For the mid-range emissions scenario IS92a and moderate change in climate factors, the "best estimate" is that global sea level will rise by 0.20 m (0.08–0.38 m) by the year 2050 and 0.49 m (0.20–0.86 m) by the year 2100. (The bracketed values are the range of uncertainties.) The lowest projections (IS92c) in Table 4.1 are similar to sea-level rise continuing at present rates as measured at major ports around New Zealand during the last 100 years. These lower projected values are coincidentally of the same order of magnitude as the variability in the sea level at seasonal to interdecadal timescales (Section 4.1). This explains the current difficulty in pinpointing any small acceleration in sea level records due to climate change.

Scenario	Climate factors	2050	2100
Linear NZ trend continues (+1.7 mm/yr)	climate trend over the 1900's continues	0.09 m	0.17 m
IS92e/high	high ice melt + 4.5°C climate sensitivity	0.39 m	0.94 m
IS92a/mid	moderate ice melt + 2.5°C climate sensitivity	0.20 m	0.49 m
IS92c/low	low ice melt + 1.5°C climate sensitivity	0.07 m	0.13 m

Table 4.1: Revised 1995 IPCC projections in sea-level rise for the years 2050 and 2100 for three different greenhouse gas emission scenarios (IS92x) and climate factors, compared with an ongoing average linear rise from last century.

The 1995 IPCC estimates of sea-level were lower than those presented in the first 1990 IPCC report, due primarily to lower predictions of global *temperature* change, which drive the projections of sea-level rise. The 1995 "best estimate" projections amount to an accelerating rate of rise in sea level relative to 1995 levels, of 2.5 mm/yr by 2030 and 5 mm/yr by 2050. At this stage, sea-level records from coastal and port gauges show no evidence yet of a statistically significant acceleration in sea-level rise (Bell et al., 2000). The forthcoming IPCC Third Assessment Report (March 2001) is unlikely to suggest any further reductions in 1995 projections for sea-level rise[2].

Explicitly or implicitly, one must convert a scenario into a probability estimate before one can decide whether the risk warrants a particular action. A thorough analysis of the risk was undertaken by the US Environmental Protection Agency, using computer models employed for previous IPCC assessments as well as subjective assessments of climate and glaciology scientists about the values for the various model coefficients

[2] From the IPCC Data Distribution Centre web site: http://ipcc-ddc.cru.uea.ac.uk/

(Titus and Narayanan, 1996). The procedure isolates the ongoing regional trend in sea-level rise from a normalised projection of global rise (due to the greenhouse effect). The latter estimates the extent to which future sea-level rise may exceed that which would have occurred if current regional trends simply continued. Table 4.2 below gives the projected regional sea-level rise for New Zealand during the present century associated with two probabilities (50% chance and a smaller 10% chance) based on the current regional trend of +1.7 mm/yr combined with the projected contribution from the greenhouse effect.

Year	50% chance that SLR will reach	10% chance that SLR will reach
2025	0.11 m	0.18 m
2050	0.20 m	0.33 m
2070	0.31 m	0.50 m
2100	0.45 m	0.74 m

Table 4.2: Projected sea-level rise (SLR) for New Zealand for two probabilities of exceedance based on the approach of Titus and Narayanan (1996) for assessing the risk associated with regional sea-level rise.

Finally, the IPCC recognise that changes in future sea level will exhibit regional variations and will not occur uniformly around the globe (Warwick et al., 1996). This poses the question as to the usefulness of a single value of a mean global rise in sea level. Further, the global rise in sea level does not take into account the relative vertical movement of the landmass at each location. The Wellington–Kapiti region contains complex faulting structures, with a recent discovery of an active offshore fault running north of Kapiti Island (Phil Barnes, NIWA, pers. comm.). Estimates of vertical movement for the Kapiti coast have been proposed by Pillans (1986), of an average +0.5 mm/yr uplift, and Gibb (1978) suggesting an uplift of ~2 m over the past 5000 years (average=+0.4 mm/yr). These values represent a significant proportion of the present sea-level rise of 1.7 mm/yr, which would reduce the relative rise in sea level to 1.2–1.3 mm/yr along the Kapiti coast. However over geological timescales, it is not clear whether this is an ongoing uplift or whether it largely occurs as co-seismic activity during seismic events. The conservative approach would be to neglect any uplift until further quantitative information comes to hand. (Note: accurate GPS loggers are being positioned on a few sea-level gauges around New Zealand to quantify vertical landmass movements.)

5. CLIMATE VARIABILITY (EL NINO AND WINDINESS)

5.1 Long-term Climate Prediction Models

A number of international centres are involved in modelling climate changes in response to changes in human-induced changes in atmospheric composition ("greenhouse gases" and sulphate aerosols). The Intergovernmental Panel on Climate Change (IPCC) has set up an internet web site (http://www.dkrz.de/ipcc/ddc/) where climate simulation results for a number of coupled atmosphere-ocean general circulation models (GCMs) are made available. For a climate forecast, we have focussed on the most commonly used emissions scenario, where the atmospheric concentration of sulphate is specified, and the carbon dioxide concentration follows historical observations up to 1989, and is thereafter compounded at 1% annually over the coming century.

5.2 Windiness Prediction

Outputs from global circulation models (GCMs) from six leading centres have been analysed, for the present-day climate and for projected future changes over the next century (Mullan et al., 2000). All models simulate most of the broad scale features of the observed present-day climate, although only four of the six produce realistic El Niño-Southern Oscillation (ENSO) patterns in the New Zealand region. For the century as a whole (1980s to 2080s), all models show a strengthening (or at least no weakening) in the westerly wind circulation over New Zealand, associated with an increase in the mean Equator to pole temperature difference (i.e., the polar regions are not expected to warm to the same extent as the equatorial regions). However, the magnitude of the change varies between models. The CSIRO GCM (Gordon and O'Farrell, 1997) shows the smallest overall variation, with a small decrease over the first 50 years, followed by a compensating increase. Other models (e.g., the UK Met Office GCM; Mitchell and Johns, 1997) show a 25% or greater increase in annual mean westerly winds.

Averaged over all GCMs, the strength of the background westerly circulation over central New Zealand is predicted to increase by around 15% over the coming 50 years, and by another 15% in the 50 years after that. Given the range of model outcomes, approximate confidence bands for the two consecutive 50–year periods are –5% to 35%, and 0% to 30%.

5.3 ENSO and Longer-term Variability

There is little agreement between models on projected changes in El Niño–Southern Oscillation (ENSO) behaviour (Mullan et al., 2000). On average, a slight shift towards

La Niña conditions is indicated, but changes in year-to-year variability are complex. For the ECHAM4 model, Timmermann et al. (1999) found a mean change towards El Niño conditions, but interspersed with frequent strong La Niña events. Other modelling centres (e.g., UK Met Office) find little change in ENSO until greenhouse gas concentrations reach four times pre-industrial levels. At present, there is no strong evidence of significant changes in ENSO, at least over the coming 50–100 years.

Recent research has indicated that the behaviour of ENSO is modulated on the 20–30 year time scale by what has become known as the "Interdecadal Pacific Oscillation" (IPO, e.g., Mantua et al., 1997; Minobe, 1999). The IPO conditions the tropical Pacific towards extended periods of predominantly El Niño conditions, followed by periods of more evenly balanced La Niña and El Niño events. The last 25 years have been dominated by El Niño conditions, resulting in an average increase in westerly winds over central and southern New Zealand, compared to the previous 30 years shown in Fig. 5.1. The degree of westerly wind conditions is represented by the atmospheric pressure difference between Auckland and Christchurch (also see http://www.niwa.cri.nz/press_releases/aug6_98.html for more information). The 1950s were also a period of enhanced westerly wind activity, which coincided with a spate of coastal erosion along the Kapiti coast (Donnelley, 1959).

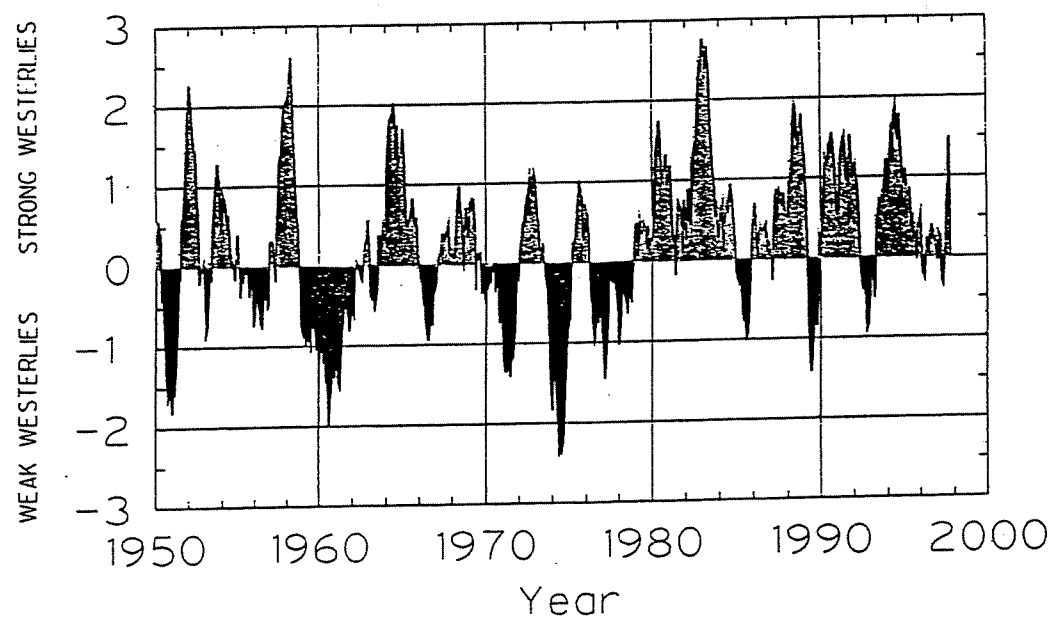

Figure 5.1: NZ climate index (Auckland–Christchurch barometric pressure) from 1950–2000. A positive index value denotes stronger westerlies, Note the IPO climate regime shift to dominant westerlies in the late 1970s from persistent El Niño events, whereas prior to that, the IPO was associated with a more even balance between El Niño and La Niña events.

The IPO may reverse over the next 2–5 years, which could bring in 2–3 decades of somewhat lighter westerlies over the country and more La Niña episodes than we have had in the past two decades. Such decadal-scale variability in the wind climate of New Zealand must be taken into account and should be seen as overlaid on the greenhouse gas-related climate changes discussed above in Section 4.2. It is also important to distinguish the difference between weather (e.g., a particular storm event) and climate, which is the background or context in which adverse weather events occur. For instance, an El Niño climate episode creates "permissible" background conditions for more westerly storms to impact the Kapiti coast, and vice versa for La Niña episodes. But severe storms can still occur during any ENSO episode.

The Interdecadal Pacific Oscillation (IPO) has also had a noticeable effect on the number and severity of storm surges (>0.1 m) in the Bay of Plenty, with fewer since the climate regime shift in 1976 (Gibb and de Lange, 2000). The likely effect of the IPO on storm surge activity (frequency and magnitude) along the Kapiti coast is unknown.

6. DESIGN STORM SET-UP AND TIDE LEVELS

The various components that can contribute to extreme sea levels along the Kapiti coast have been discussed separately above. The quantitative estimation of extreme sea levels and their return period becomes a difficult exercise, given the paucity of long-term sea level and wave information for the coast. The various components that contribute to extreme levels cannot simply be added together to form a "worst case" scenario e.g., the highest tide this century + biggest storm surge + La Niña conditions + heavy seas. Such a combination would have an extremely small joint probability of occurrence meaning it is of no practical use. The approach we have taken is to combine less extreme conditions for each component into a realistic extreme sea level for Waikanae Beach, to which the projected climate change factors (sea-level rise and windiness) can be added. Extreme sea levels at other localities along the Kapiti coast can be varied according to tide range differences and wave run-up exposure.

In this section, extreme sea levels are converted to the geodetic Wellington MSL Datum–1953 (WD-53), on the basis that the mean level of the sea (MLOS) over the past decade or so has been approximately 0.16 m above WD-53.

Storm surge

In the 50 years since 1950, the September 1976 event stands out as the highest known storm surge along the Kapiti coast, estimated at ~0.7 m (Gibb, 1978). Minimum daily barometric pressures at or below 975 hPa have occurred 4 times at Paraparaumu

Airport since 1962. Such events produce an inverted barometer set-up of just over 0.4 m in sea level. If such a low-pressure events were to coincide with strong onshore mean wind speeds of >38 knots (19.7 m/s), similar to those experienced in the September 1976 event, the wind stress set-up component would typically be 0.2–0.25 m. Such wind events from the west round to NNW occurred 12 times in a 20-year period 1975–1995 (S. Reid, pers. comm.). Considering both wind speed and barometric pressure for these 12 events, the September 1976 event stands out clearly. The next highest cluster of storm surge set-up's for the 20-year period are estimated to have been about 0.4–0.45 m, because the minimum barometric pressure was higher and the wind duration was much shorter than the 1976 event.

Fortunately the coastal shelf is relatively narrow off Kapiti, with the seabed falling to depths of >50 m about 5–7 km offshore, which constrains the growth of wind-stress set up. Combined together, the total storm surge for an infrequent combination would yield a storm surge of similar proportions to the 1976 event or around 0.75 m set-up to be conservative, given the lack of sea-level data.

Given the historic analysis above (Section 3.4), a storm surge of 0.7 m would therefore appear to have a reasonably low annual exceedance probability (AEP) of around 2% for the Kapiti coast. That means there is only a 2% chance of such a storm surge being exceeded in any one year, or a 50–year return period. This is confirmed by evidence of other recorded storm surges around New Zealand, being up to 0.7–0.9 m at estimated return periods of 50–100 years. For example, a 0.88 m maximum storm surge was recorded in Tauranga during Cyclone *Giselle*, which ranks about 2nd in severity since 1890 (Bell et al., 2000; Gibb and de Lange, 2000). Based on extrapolating from the limited sea-level databases and visual observations, the upper limit for storm surges in New Zealand appears to be ~1 m (Bell et al., 2000). The AEP for such an event would be considerably lower than 1% i.e., a return period of at least 100 years.

Therefore adopting conservative values, a storm surge set-up of 0.85 m (excluding wave set-up and run-up) would be a reasonable estimate of a 1% AEP and 0.75 m set-up for a 2% AEP for Kapiti, until a longer sea-level record is accumulated.

High tide levels

MHWS, calculated by adding the lunar M_2 and solar S_2 amplitudes (half-range), represents the high tide level that is exceeded by ~10% of all high tides. MHWS for the Kapiti Island sea-level recorder is 1.06 m above WD-53. The high astronomical tide (HAT), exceeded by only 1% of high tides, is 1.16 m above WD-53, while the most extreme high tide this century will be 1.27 m above WD-53. These levels also apply to Waikanae Beach on the Kapiti coast, directly east of the recorder.

For the purpose of establishing combined tide and storm surge design levels, the 1% and 2% AEP storm surges are combined with the HAT (1.18 m above WD-53) and MHWS (1.06 m above WD-53) respectively. This is also consistent with the 1957 storm-surge event, which occurred on top of a MHWS tide, while the 1976 event that occurred on a lesser high tide (0.9 m).

The implication of the considerable spatial variation of tides along the Kapiti coast is that estimates of extreme tides made using data from the sea-level recorder on Kapiti Island need to be scaled to obtain the corresponding high-water level along the coast. Thus, extreme high tides to the north (Otaki Beach) need to be scaled up by as much as 112% and those to the south (Pukerua Bay) need to be scaled down by as little as 68% (see Table 3.1).

Wave set-up and run-up

The only known estimate of the combined wave set-up and final run-up (that occurs landward of the breaker zone) is the observation by Gibb (1978) of an average of 2.6 m vertical shift in the driftwood line during the September 1957 storm. Wave set-up is dependent on the breaking wave height, wave period and also the beach and nearshore slope. Generally wave set-up alone is approximately 8–15% of the incident breaking wave height, depending on the nearshore bed slope, being the lesser value for steeper seabed slopes.

For example, consider regular breaking waves with a 10 second period approaching normal to the Kapiti coast with a typical nearshore slope of 0.02 (1 on 50). Estimated deepwater significant wave heights of 5 m and 6 m (for 50 and 100 year return periods) could produce a 0.75 m and 0.9 m wave set-up respectively at the shoreline, based on the method outlined in CERC (1984). However natural waves at the coastline exhibit "groupiness" or a surf-beat, where a group of larger waves is followed by smaller waves and so on. These groups of larger waves may pump significant quantities of seawater towards the shore, so a further 0.1 m was added to the above wave set-up values calculated for regular waves.

Wave run-up is difficult to quantify for a stretch of coast, as it is strongly dependent on the site-specific beach and foredune profiles and the associated substrate (e.g., walls, rocks, gravel, sand) at each site. Therefore a site-by-site appraisal is needed for each section of coastline.

Sea-level variability

Taking into account longer records from elsewhere in New Zealand, the interannual elevation of background sea level at Kapiti could peak at +0.15 m for a month or so during strong La Niña episodes and in warmer summer months. For the purposes of a

combined design storm-surge event, a nominal +0.1 m set-up should be added to both the 1% and 2% AEP design levels to account for elevated seasonal and La Niña sea levels.

Climate change (windiness and sea-level rise)

There is a 50% chance that sea level around New Zealand will rise by +0.20 m by 2050 and by +0.45 m by 2100, according to the 1995 IPCC estimates. Forthcoming IPCC projections (due out in March 2001) are unlikely to recommend any lower rates of sea-level rise due to greenhouse effects.

While ENSO episodes are not expected to change significantly, the global circulation models are predicting a 15% increase in windiness for the next 50 years, and by another 15% for 50 years after that. What effect this will have on the magnitude and frequency of extreme storms is still unclear.

The Interdecadal Pacific Oscillation (IPO) may reverse over the next 1–5 years, which could bring in 2–3 decades of somewhat lighter "background" westerlies over the country and more La Niña episodes than we have had in the past two decades, which will elevate regional sea levels above normal. However, storms generated by deep depressions are likely to happen at any time.

Design high water levels

Combining the above estimates, the following design high water levels for a 1% and 2% AEP, relative to the tide range at Waikanae Beach, are proposed.

Table 6.1: Design high water levels, comprising various set-up components, for 2% and 1% AEP (50 and 100 year return periods) applicable to the tide range at Waikanae Beach. Bold values are relative to Wellington MSL Datum (1953) or WD-53. The projected sea-level rise for 2050 is assigned to the 2% AEP level and the 2100 projected rise is added to the 1% AEP level. Wave run-up requires a site-by-site consideration of beach and foredune slopes and substrate conditions.

Factor	2% AEP (m set-up) (bold in m above WD-53)	1% AEP (m set-up) (bold in m above WD-53)
Storm surge set-up	+0.75	+0.85
High tide*	**1.06**	**1.18**
ENSO (La Niña)	+0.10	+0.10
Sub-total	**1.9**	**2.1**
Wave set-up	+0.85	+1.00
Sub-total	**2.8**	**3.1**
Sea-level rise (2050, 2100)	+0.20	+0.45
Sub-total	**3.0**	**3.5**
Windiness	?	?
Wave run-up	Site by site	Site by site

* Because tide range reduces with distance south, could apply % factor at sites away from Waikanae, of up to 112% for Otaki Beach and as small as 68% for southern Pukerua Bay.

7. CONCLUSIONS AND SUMMARY

Wave conditions off the Kapiti Coast have been assessed. There are no in situ measurements and a programme is recommended for measuring waves and currents near the shore. Such data are required to verify the local wave conditions, and to assess alongshore drift.

Modelling the local wave growth has generated new wave information. A 20-year record was synthesised from a time series of representative winds. Corresponding time series for ten shallow water sites along the coast were inferred by applying a refraction model.

Analyses of known historic storm events, a 3-year sea-level record from Kapiti Island and nearly 30 years of barometric pressure data from Paraparaumu Airport have also been completed. The main findings are:

- Wave heights rarely exceed 3 m. The highest deep-water significant wave height estimated for waves off the Kapiti Coast was 4.5 m in early November 1995, followed by 4.1 m in March 1995.

- Waves refract into the coast, but a large proportion of their energy reaches the 10-m isobath.

- Swell from Cook Strait and the Tasman Sea may reach the Kapiti Coast, but it is substantially attenuated, with less than 15% of the energy reaching the coast.

- During the major event of 11-13 September 1976, estimated H_s offshore reached 3.6 m with a peak period of 9.4 s.

- Highest observed storm surge was 0.7 m set-up accompanied by a 2.6 m wave set-up and run-up in the 11–13 September 1976 storm (Gibb, 1978);

- Lowest recorded barometric pressure of 973 hPa would have produced an inverted barometer set-up of just over 0.4 m due to pressure alone (excluding winds);

- The highest predicted high tide for next 100 years will be 1.27 m above Wellington MSL Datum (1953);

- Tide range reduces as one moves south along the Kapiti coast, so high tides to the north (Otaki Beach) need to be scaled up by as much as 112% and those to the south (Pukerua Bay) need to be scaled down by as little as 68%;

- The interannual (year-to-year) elevation of background sea level at Kapiti could peak at +0.15 m for a month or so during strong La Niña episodes and warmer summer months. For the purposes of a combined design storm-surge event, a nominal +0.1 m set-up should be added to both the 1% and 2% AEP design levels;

- There is a 50% chance that sea level around New Zealand will rise by +0.20 m by 2050 and by +0.45 m by 2100, according to the 1995 IPCC estimates. Forthcoming IPCC projections (due out in March 2001) are unlikely to recommend any lower rates of sea-level rise due to greenhouse effects;

- While ENSO episodes are not expected to change significantly, the global circulation models are predicting a 15% increase in windiness for the next 50 years, and by another 15% for 50 years after that. What effect this will have on the magnitude and frequency of extreme storms is still unclear;

- Design sea-level set-up for 2% AEP (50-year return period) and 1% AEP (100-year return period) scenarios are estimated to be 3 m and 3.5 m respectively above Wellington MSL Datum (1953) for Waikanae Beach. An additional factor for wave run-up needs to be included on a site-by-site basis, plus the tidal range factor for beaches north and south of Waikanae Beach. No account has been included for a predicted increase in windiness over the next 100 years.

It is recommended that a measurement programme be undertaken to validate the synthetic wave record assumed in this study. This would be best served by deploying a directional system, such as an S4 current meter, in about 10m water off the most vulnerable location (Raumati) for at least 6 months.

8. ACKNOWLEDGEMENTS

We acknowledge the help of John Marks (Wellington Regional Council), and Westgate Transport Ltd. for providing Port of Taranaki sea-level data.

9. REFERENCES

Bell, R.G.; Goring, D.G. (1997). Low-frequency sea-level variations on the northeast coast, New Zealand. In: Proceedings of 13th Australasian Coastal & Ocean Engineering Conference, Christchurch, Vol. 2: 1031–1035.

Bell, R.G.; Goring, D.G.; de Lange, W.P. (2000). Sea-level change and storm surges in the context of climate change. *IPENZ Transactions 27(1)/Gen*: 1–10. Also at web site: http://www.ipenz.org.nz/knowledge/transactions/transactions2000/general/contents.htm

Black, K.P. and Rosenberg, M.A. (1992a). Natural stability of beaches around a large bay. *Journal of Coastal Research*. 8(2): 385-397.

Black, K.P. and Rosenberg, M.A. (1992b). Semi-empirical treatment of wave transformation outside and inside the breaker line. *Coastal Engineering*. 16: 313-345.

Black, K.P. (1995) The hydrodynamic model 3DD and support software, Occasional Report 19, Department of Earth Sciences, University of Waikato, New Zealand.

Black, K.P. (1997) Wave refraction model WBEND. Occasional Report, Joint Centre of Excellence in Coastal Oceanography and Marine Geology, Department of Earth Sciences, University of Waikato, New Zealand.

CERC (1984). Shore Protection Manual. US Corps of Engineers, Dept. of the Army, Vol. 1. Fourth edition.

Donnelly, L.S. (1959). Coastal erosion: Paekakariki to Waikanae–Hutt County. *NZ Engineering*, February 15, 48–52.

Ewans, K. C.; Kibblewhite, A. C. (1990): An examination of fetch limited wave growth off the West Coast of New Zealand by a comparison with the JONSWAP results. *Journal of Physical Oceanography 20*: 1278-1296.

Foreman, M.G.G. (1977). Manual for tidal heights analysis and prediction. Pacific Marine Science Report No. 77-10. Institute of Ocean Sciences, Patricia Bay, Victoria. B.C., Canada. 101 p.

Gibb, J.G. (1978). The problem of coastal erosion along the "Golden Coast", Western Wellington, New Zealand. *Water & Soil Technical Publication No. 10*, Water & Soil Division, Ministry of Works and Development, Wellington. 19 p.

Gibb, J.G.; de Lange, W.P. (2000). Storm surges at Tauranga. *New Zealand Journal of Marine and Freshwater Research*. In press

Goring (1995). Short-term variations in sea level (2–15 days) in the New Zealand region. *New Zealand Journal of Marine and Freshwater Research 29*: 69–82.

Gorman, R.; Laing, A.K. (2000): Bringing wave hindcasts to the New Zealand coast. *Journal of Coastal Oceanography.*

Hannah, J. (1990). Analysis of mean sea level data from New Zealand for the period 1899–1988. *Journal of Geophysical Research 95(B8)*: 12,399–12,405.

Harris, T.F.W. (1990): Greater Cook Strait, Form and Flow. DSIR Marine and Freshwater, Wellington. 212 p.

Hasselmann, K., et al., (1973): Measurements of wind wave growth and swell decay during the Joint North Sea Wave Project (JONSWAP). *Deutchen Hydrographischen Zeitschrift,* Suppl. A8, No12.

Hasselmann, K., Ross, D.B, Muller, P. and Sell, W., (1976): A parametric wave prediction model. *Journal of Physical Oceanography.* 6:200-228.

Hutt, J.A. (1997) Bathymetry and wave parameters defining the surfing quality of 5 adjacent reefs. MSc thesis. Joint Centre of Excellence in Coastal Oceanography and Marine Geology, Earth Sciences Department, University of Waikato. 170 pp.

Kibblewhite, A. C.; Berquist, P. R.; Foster, B. A.; Gregory, M. R.; Miller, M. C. (1982): Maui development environmental study. Report on phase two 1977-1981. University of Auckland for Shell BP and Todd Oil Services Ltd, Auckland. 174 p.

Laing, A. K. (1985): An assessment of wave observations from ships in Southern Oceans. *Journal of Climate and Applied Meteorology 24*: 481-494.

Laing, A.K. (1994): Features of marine wind fields over New Zealand waters from ERS-1 scatterometer data. *N. Z. J. Marine and Freshwater Research 28(4)*: 365-378.

Laing, A.K.; Brenstrum E. (1996): Scatterometer observations of low-level wind jets over New Zealand coastal waters. *Weather and Forecasting 11*(4): 458-475.

Laing, A.K., (2000a): The New Zealand wave climate from satellite observations. *N. Z. J. Marine and Freshwater Research 34*(4) - in press.

Laing, A.K., (2000b): Rapid onset of waves on the east coast of New Zealand. *Journal of Coastal Oceanography* - in press.

Laing, A.K.; Gorman R. (2000): The ocean wave climate around New Zealand from satellites and models. *Water and Atmosphere 8(1),* 20-23.

Mantua, N.J.; Hare, S.R.; Zhang, Y.; Wallace, J.M.; Francis, R.C. (1997): A Pacific interdecadal climate oscillation with impacts on salmon production. *Bulletin American Meteorological Society 78*: 1069–1079.

McComb, P., Black, K.P. and Atkinson, P. (1997): High-resolution wave transformation on a coast with complex bathymetry. Pacific Coasts and Ports'97, Christchurch, 7-11 September 1997.

Minobe, S. (1999). Resonance in bidecadal and pentadecadal climate oscillations over the North Pacific: Role in climatic regime shifts. *Geophysical Research Letters 26(7)*: 855–858.

Mitchell, J.F.B.; Johns, T.C. (1997)" On modification of global warming by sulfate aerosols. *Journal of Climate 10*: 245–267.

Mullan, A.B.; Wratt, D.S.; Renwick, J.A. (2000): Transient model scenarios of climate changes for New Zealand. *Weather and Climate*, submitted.

Nunn, P.D. (1998). Sea-level changes over the past 1000 years in the Pacific. *Journal of Coastal Research 14*: 23–30.

Pielke, R.A., W.R. Cotton, R.L. Walko, C.J. Tremback, W.A. Lyons, L.D. Grasso, M.E. Nicholls, M.D. Moran, D.A. Wesley, T.J. Lee, and J.H. Copeland, (1992): A comprehensive meteorological modelling system - RAMS. *Meteor. Atmos. Phys.*, 49, 69-91.

Reid, S. J.; Collen, B. 1983: Analysis of wave and wind reports from ships in the Tasman Sea and New Zealand areas. *New Zealand Meteorological Service Miscellaneous Publication 182*. 74 p

Timmermann, A.; Oberhuber, J.; Bacher, A.; Esch, M.; Latif, M.; Roeckner, E. (1999). Increased El Niño frequency in a climate model forced by future greenhouse warming. *Nature* 398: 694–697.

Titus, J.G.; Narayanan, V. (1996). The risk of sea level rise. *Climatic Change 33*: 151–212.

Walters, R.A.; Goring, D.G.; Bell, R.G. (in press). Ocean tides around New Zealand. *New Zealand Journal of Marine and Freshwater Research* (accepted).

WAMDIG (the WAM Development Group - Hasselmann, S. et al), (1988): The WAM Model - a third generation ocean wave prediction model. *Journal of Physical Oceanography 18*(12): 1775-1810.

Warwick, R.A.; Le Provost, C.; Meier, M.F.; Oerlemans, J.; Woodworth, P.L. (1996): Changes in sea level. *In:* Houghton, J. T.; Meira Filho, L.G.; Callander, B.A.; Harris, N.; Kattenberg, A.; Maskell, K. *eds* Climate change 1995: The Science of climate change, pp. 359–405. Cambridge University Press, Cambridge.

Williams, Gordon, H. B. and S. P. O'Farrell, (1997): Transient climate change in the CSIRO coupled model with dynamic sea ice. *Monthly Weather Review*, **125**, 875-907.